Optimal Gaits for Dynamic Robotic Locomotion

Jorge Cortés* Sonia Martínez* James P. Ostrowski†
Kenneth A. McIsaac†

September 6, 2001

Abstract

This paper addresses the optimal control and selection of gaits in a class of dynamic locomotion systems that exhibit group symmetries. We study near-optimal gaits for an underwater eel-like robot, though the tools and analysis can be applied more broadly to a large family of nonlinear control systems with drift. The approximate solutions to the optimal control problem are found using a truncated basis of cyclic input functions. This generates feasible paths that approach the optimal one as the number of basis functions is increased. We describe an algorithm to obtain numerical solutions to this problem and present simulation results that demonstrate the types of solutions that can be achieved. Comparisons are made with experimental data using the REEL II robot platform.

1 Introduction

Biological organisms use an interesting and varied set of motion patterns, or ***gaits***, to move themselves through their environment. In fact, many organisms choose from a finite, though parameterized, set of gaits, depending on several factors, including the gait's appropriateness for the terrain and its efficiency within a particular operating regime [3, 24]. Many different forms of locomotion have been studied from both biological and robotic perspectives. Along with wheeled mobile platforms and legged locomotion, other forms of robotic (and biological) locomotion that have been studied

---

*Laboratory of Dynamical Systems, Mechanics and Control, Instituto de Matemáticas y Física Fundamental, CSIC, Serrano 123, Madrid 28006, SPAIN, (j.cortes@imaff.cfmac.csic.es, s.martinez@imaff.cfmac.csic.es)

†General Robotics, Automation, Sensing and Perception Laboratory, University of Pennsylvania, 3401 Walnut Street, Philadelphia, PA19104-6228, USA, (jpo@grasp.cis.upenn.edu, kamcisaa@seas.upenn.edu)

include snake-like motions [11, 25, 39], inchworm motions [26], and even the motion of water-bugs [23] and paramecia [27, 29, 46]. In all these systems, the dynamics of the system are subject to nonholonomic constraints and the system relies on oscillatory, phased inputs to generate any desired (even uniform) motion. This class of ***undulatory locomotion systems*** also includes less obvious forms of locomotion, such as the reorientation of a satellite using internal rotors [7, 31, 44, 56], the reorientation of a falling cat [21, 42], finger gaiting (in grasping), and the movement of underwater and aerial vehicles [10, 14, 34, 39, 58]. Such undulatory locomotion systems have many potential applications, for example, in the actuation of underwater robots and micro-robots.

In the area of optimal controls, early work by Bailleuil [4] took a geometric viewpoint in studying control and motion planning. Brockett [8, 9] derived the optimal controls for a special class of driftless nonholonomic systems and showed that the optimal input patterns can be described by sinusoidal and elliptical functions. Walsh, Montgomery, and Sastry [52, 56] also studied the motion planning problem for nonholonomic systems, by focusing on systems that evolve on a Lie group. More recently, Ostrowski [46] for driftless systems, and Koon and Marsden [30] (see also Cortés and Martínez [12]) for dynamic systems, have investigated optimal control of nonholonomic mechanical systems that exhibit group symmetries and derived a set of simplified necessary conditions for the control inputs.

Since it is very difficult to obtain analytical solutions for the optimal controls except in extremely simple cases, it is beneficial to pursue numerical solution techniques. We briefly survey some of the work in this area, specifically in the context of nonholonomic locomotion systems. Some of the original work is due to Dubins [19] and Reeds and Shepp [51] who studied the optimal motion of a car-like vehicle with and without a forward velocity constraint, respectively (see also [5, 54] for interesting revisitations of the problem). Laumond *et al.* [33] describe an algorithm for planning near minimum distance trajectories for a nonholonomic car moving among obstacles. Work by Kumar and others [18, 57] has studied optimal control techniques to determine the control inputs for nonholonomic systems, while avoiding obstacles (modeled as inequality constraints) and optimizing a suitable cost function such as energy consumption. Since these methods incorporate the full system dynamics, the optimal solutions include the feedforward actuator force/torque inputs, as well as the state space trajectories. In [50], Ostrowski, Desai, and Kumar studied the use of these techniques applied to robotic locomotion systems, demonstrating their application to the snakeboard system. They were able to show the possibility of gait transitions and motion planning for dynamic nonholonomic systems; however, the computational cost of solving the optimal control problem using these techniques is quite expensive.

Our current work seeks to strike a balance between generating the motion plans using simple, un-optimized input sets and solving the full optimal control problem for a relatively unrestricted class of inputs. Thus, the oft-cited work of Murray and Sastry [43] is important, since this found an early use of sinusoids as sub-optimal inputs for solving the steering problem for nonholonomic systems. A similar setting is used by Leonard and Krishnaprasad [35] to study the motion control and planning problem for systems on Lie groups. Ostrowski and Burdick [49] (and later [40]) discuss a variety of control plans for such systems by investigating different sinusoidal input motions of the shape variables, which were termed "gaits". These led to a set of open-loop, feedforward motion primitives that can then be incorporated into a feedback control scheme [40].

Closest to the current work is that of Fernandes, Gurvits, and Li [21, 22], who solved for *near optimal* solutions for the "locomotion" problem of the falling cat. They proposed a mechanism for choosing the control input as a linear combination of smooth orthonormal basis functions. This is the same principle which we have applied to the current context, and we note that much of the analysis presented here fundamentally is based on developing suitable extensions to [22] to deal with systems with drift. In fact, although Fernandes *et al.* limited the applications they described to driftless nonholonomic systems, the techniques can be seen to have a fairly broad application to nonlinear control systems, including those with drift, in which the inputs can be chosen to be cyclic in nature.

In this paper, we focus our attention on developing optimal controls for two large classes of locomotion problems that can be described within the same unifying framework. On the one hand, we consider locomotion systems whose interaction with the environment is modeled by some linear constraints $\omega^1, \dots, \omega^k$ such that the trajectories of the system must satisfy $\omega^j_a(q)\dot{q}^a = 0$, for $1 \leq j \leq k$. The example of the snakeboard mentioned before [36, 45] is a paradigm of this large class of systems. On the other hand, we also treat the problem of snake and eel-like robotic locomotion, where the interaction of the system with the environment is via either viscous or fluid drag forces acting on the body. In this respect, we discuss specifically ***anguilliform***, or eel-like, locomotion. We build on our previous work on locomotion [45, 49], where we used tools from differential geometry to simplify the analysis of nonholonomic dynamic systems with group symmetries. We formulate the optimal control problem for these systems in a manner that is easy to compute. There is a substantial body of literature in biological, undulatory locomotion systems (see, for example, [2, 3, 16]) that suggests that such systems may select gaits and switch between gaits in order to minimize the energy expended during locomotion. Motivated by this, we study the optimal gaits that minimize the energy expenditure for the system, in our case an eel robot. We also contrast the resulting near-optimal solutions with those that have been generated previously in the literature without regards to optimization, using constructive, open-loop techniques [39, 40].

The outline of the paper is the following. In Section 2, we describe the mathematical formulation of nonholonomically constrained and eel-like robotic locomotion. As an example, we introduce the underwater REEL II robot. In Section 3, we discuss the unifying framework for both types of locomotion. In Section 4, we present the *Basis Algorithm* for control systems with non-zero drift, as an extension of the work in [22], to solve numerically the optimal control problem for these systems. Section 5 contains several simulations for the REEL II robot, where in some of them we have contrasted this approach with previous work on open-loop gaits [39]. We also present experimental results and based on our experience discuss the effectiveness of these techniques for use in real experimental platforms. Finally, we have gathered in the Appendix the proof of the convergence of the *Basis Algorithm* under Bounded Input, Bounded State (BIBS) stability.

2 Lagrangian dynamics and the reduction process

Both nonholonomically constrained locomotion and eel-like robotic locomotion can naturally be formulated in the context of dynamic mechanical systems, and so are governed by Lagrange's equations. In this section, we review the well-suited framework developed for them elsewhere. We refer the reader to [6, 39, 45, 49] for a more thorough discussion on the derivation of the equations.

Let Q be an n-dimensional manifold, describing the set of all possible configurations of the locomotion system. We assume the existence of a Lagrangian function, $L(q, \dot{q})$, governing the dynamics of the system, which is usually given by its kinetic energy. When studying locomotion systems, it is important to note that the configuration manifold, Q, can always be divided into two parts: the ***position*** (and ***orientation***) of the body and the internal ***shape*** of the system (see [26, 49]). The position space of the body will generally be a Lie subgroup of $SE(3)$; for example, $SE(2)$ for a snake or paramecium, $SE(2) \times \mathbb{R}$ for a blimp, or $SO(3)$ for a satellite or the falling cat. The remaining configuration variables of the system represent the internal shape and constitute the ***shape space*** M. In the standard mathematical nomenclature, $Q = M \times G$ is called a ***trivial principal fiber bundle*** with ***base space*** M and ***fiber*** G. The configuration space Q is "trivial" because the product structure is global, and it is a "principal" bundle because the fiber is a Lie group. The Lie group structure (which is common to *all* locomotion systems) allows us to develop a systematic method, called ***Lagrangian reduction***, for reducing the equations of motion to a more compact form [6, 45, 49].

In working with the Lie groups $SE(2)$ and $SE(3)$, we use a homogeneous matrix representation, so that the group action becomes simply matrix multiplication. An element $g \in G$ thus represents the transformation between an inertial or ground frame and a frame attached to the moving body. Associated with a Lie group, G, is its ***Lie algebra***, $\mathfrak{g}$, which can be identified with the tangent space at the identity, T_eG. The elements of the Lie algebra associated with $SE(2)$ or $SE(3)$ represent a reduced velocity, and are the twists encountered in screw theory. In particular, we will be interested in ***body*** velocities (that is, velocities taken in a body-fixed frame), where an element $\xi \in \mathfrak{g}$ is defined as $\xi = g^{-1}\dot{g}$. This is in contrast to ***spatial*** velocities, represented by $\xi^s = \dot{g}g^{-1}$, taken in an inertial frame. The distinction arises naturally due to the non-Abelian (non-commutative) nature of matrix multiplication on the Lie group. This fact can also be observed in the nonvanishing of the so-called ***structural constants*** of the Lie algebra, defined as follows: let $e_1, \ldots, e_k$ be a basis of $\mathfrak{g}$, then the structure constants c_{ab}^c are given by the equation

$$[e_a, e_b] = c_{ab}^c e_c \, .$$

The relation between the body and the spatial velocities is given by $\xi^s = \dot{g}g^{-1} = g(g^{-1}\dot{g})g^{-1} = g\xi g^{-1} = Ad_g \xi$, where $Ad : G \times \mathfrak{g} \longrightarrow \mathfrak{g}$ denotes the ***adjoint action*** of the Lie group on its Lie algebra (see, for instance, [37]).

Conservation laws naturally arise when a Lagrangian remains fixed under the action of a Lie group G and there is no external forcing. More formally, let the action of $g \in G$ on $q = (r, h) \in M \times G = Q$ be given as $\Phi_g(r, h) = (r, gh)$, where gh represents the multiplication of G. The Lagrangian function is said to be ***G-invariant*** if $L(\Phi_g(q), D_q\Phi_g v_q) = L(q, v_q)$ for all $g \in G$ and $(q, v_q) \in TQ$. The physical interpretation of G-invariance is that the Lagrangian is invariant with respect to changes in the body-fixed frame (i.e., changes in the position and orientation of the body with respect to an inertial frame). This property implies that we can consider the ***reduced Lagrangian*** ℓ given by $\ell(r, \dot{r}, \xi) = L(r, e = g^{-1}g, \dot{r}, \xi) = L(r, g, \dot{r}, g\xi)$. The body momentum is then defined by $p = \frac{\partial \ell}{\partial \xi}$, which is related to the spatial momentum p^s via $p = Ad_g^* p^s$, where $Ad_g^* : \mathfrak{g}^* \longrightarrow \mathfrak{g}^*$ is the dual mapping of Ad_g, that is, $< Ad_g^*(\mu), \xi >=< \mu, Ad_g(\xi) >$ for $\xi \in \mathfrak{g}$ and $\mu \in \mathfrak{g}^*$.

For all unconstrained systems that admit group symmetries, Noether's theorem [1] states that the invariance of the Lagrangian implies a momentum conservation law, $\dot{p}^s = 0$. In other words, the system has a first integral, for example, conservation of linear and angular momentum. Examples of "locomotion" systems that obey these laws are the falling cat and the satellite with rotors [32, 42]. In body coordinates, it can be shown [47, 45] that the reduced Lagrangian ℓ can be written as

$$\ell = \frac{1}{2}(\xi^T, \dot{r}^T) \begin{pmatrix} I(r) & I(r)\mathsf{A}(r) \\ \mathsf{A}^T(r)I(r) & m(r) \end{pmatrix} \begin{pmatrix} \xi \\ \dot{r} \end{pmatrix} ,$$

and the equations of motion take the form

$$\xi = g^{-1}\dot{g} = -\mathsf{A}(r)\dot{r} + I^{-1}(r)p \, , \tag{1}$$

$$\dot{p} = ad_\xi^* p \, , \tag{2}$$

$$M(r)\ddot{r} = -C(r, \dot{r}) + N(r, \dot{r}, p) \, . \tag{3}$$

Here $ad : \mathfrak{g} \times \mathfrak{g} \longrightarrow \mathfrak{g}$ denotes the adjoint action of the Lie algebra onto itself, $ad_{e_a} e_b = c_{ab}^c e_c$ and $ad^* : \mathfrak{g} \times \mathfrak{g}^* \longrightarrow \mathfrak{g}^*$ corresponds to the associated dual map, $ad_{e_a}^* e^b = c_{ac}^b e^c$, where $e^1, \ldots, e^k$ is the dual basis of $e_1, \ldots, e_k$. $\mathsf{A}(r)$ is called the "local form" of the ***mechanical connection*** and I is the ***locked inertia tensor***. $I(r)$ describes the total inertia of the system when all joints are frozen at configuration r. The mechanical connection plays a central role in understanding locomotion [49]. Its importance stems from the fact that it determines the robot's motion as a combination of momentum, p, and internal shape changes, $(r, \dot r)$. Hence, *the connection will determine how internal shape changes create a net robot motion.* Notice also that the term $\mathsf{A}(r)$ is a function of the shape, r, only. In fact, the symmetries imply that g factors out of the system completely, since this variable enters only once, on the left-hand side of Eq. 1. Note also that if we write $\xi = \xi^a e_a$, $p = p_a e^a$, then Eq. 2 takes the form $\dot p = \xi^a c^b_{ac} p_b e^c$, and further substituting ξ^a by $-\mathsf{A}^a_\alpha \dot r^\alpha + I^{ab} p_b$ (cf. Eq. 1), we get

$$\dot p = \dot r^\alpha \left(-\mathsf{A}^a_\alpha c^b_{ac} e^c\right) p_b + p_d \left(I^{ad} c^b_{ac} e^c\right) p_b \,. \tag{4}$$

In anguilliform locomotion external forces have to be taken into account. In fact, the ability to locomote is generated through the frictional force terms. The choice of friction models allows us to model different types of snake-like (land-based or aquatic) locomotion. Using a fluid drag model, we can simulate the effect of an eel swimming. Using a viscous friction model, we can approximate the motion of a snake traveling over a smooth surface. We do not enter here into the details of modeling the different types of frictional forces. The interested reader is referred to [20, 39] for a complete discussion. A key observation is that for both of these models, the frictional forces F are invariant under the action of the Lie group, thus allowing us to incorporate them into the reduction process. Denoting $\tau(r, \dot r, \xi) = F(r, g^{-1}g, \dot r, g^{-1}\dot g)$, the momentum equation takes the form

$$\dot p = ad^*_\xi p + \tau(r, \dot r, \xi) \,.$$

Expanding $ad^*_\xi p$ as we did in Eq. 4, one can find that the equations of motion read

$$g^{-1}\dot g = -\mathsf{A}(r)\dot r + I^{-1}(r) p \,, \tag{5}$$

$$\dot p = p^T \sigma_{p\dot r}(r) \dot r + \frac{1}{2} p^T \sigma_{pp}(r) p + \tau(r, \dot r, \xi) \,, \tag{6}$$

$$M(r)\ddot r = -C(r, \dot r) + N(r, \dot r, p) + \tau_r \,, \tag{7}$$

where τ_r corresponds to the actuators that act internally to change the shape of the system.

We also note that for nonholonomically constrained locomotion systems, the conservation laws must be modified to account for the effect of constraint forces. These effects are seen in examples such as the snakeboard [36, 45, 48], which can build up momentum even though the forces of constraint do no work on the system. The equations that result from the reduction process [6] are analogous with those seen in the unconstrained case, with the exception that the momentum is no longer fixed, but may vary, depending on the internal shape. If we further assume that forces only act internally to change the shape of the system, the reduced equations of motion are

$$g^{-1}\dot g = -\mathbb{A}(r)\dot r + \mathbb{I}^{-1}(r) p \,, \tag{8}$$

$$\dot p = \frac{1}{2} \dot r^T \sigma_{\dot r \dot r}(r) \dot r + p^T \sigma_{p\dot r}(r) \dot r + \frac{1}{2} p^T \sigma_{pp}(r) p \,, \tag{9}$$

$$M(r)\ddot r = -C(r, \dot r) + N(r, \dot r, p) + \tau_r \,. \tag{10}$$

The derivation of Eq. 9, known in the literature as ***nonholonomic momentum equation***, is beyond the scope of this paper (see [6]). Roughly speaking, we can say that the right-hand side of Eq. 9 contains the expression for $ad^*_\xi p$ obtained in Eq. 4, plus several terms related to the interaction between the constraints and the symmetry directions. Eq. 10 describes the control inputs required to produce changes in the shape variables. An important part of this formulation is the definition of a ***nonholonomic momentum***, p, that describes the momentum of the system along the unconstrained directions. Eq. 9, called the ***nonholonomic momentum equation*** [6], models the evolution of the nonholonomic momentum with changes in the shape space. Finally, Eq. 8 describes the changes in position (and orientation) of the locomotion system. The ***nonholonomic connection***, $\mathbb{A}$, plays a similar role as above by formally expressing the intuitive relationships between internal shape changes $\dot{r}$ and their effect on locomotion $\xi = g^{-1}\dot{g}$.

Geometric methods for developing optimal controls for systems of the form given by Eq. 8–10 are discussed in [12, 30, 46]. In this paper, we shall address the optimal control problem from a numerical perspective, as we outline in Section 4. In contrast to [50], which also used a numerical approach, we study optimal gaits generated by means of a fixed, finite basis.

2.1 The robotic eel

The robotic eel, or REEL II, robot [39] consists of five rigid links with servo-motors as the joint actuators. The set of joint angles is transmitted to the robot by radio control and the REEL II is untethered and contained in waterproof casing, see Fig. 1. The robot was built to be used as a platform to test various locomotive gaits, such as forward, backward, turning in place and coiling gaits (see [39]) and to provide a tool for the further study of the motion planning problem for undulatory locomotion.

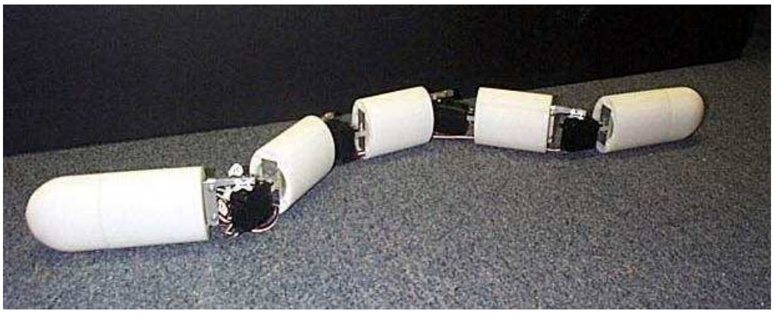

Figure 1: The REEL II robot.

We have performed the simulations presented in Section 5 for the five link model of the eel, since it is the one which corresponds to the REEL II robot. The model consists of a planar, serial chain of 5 identical links of length $2d$, mass m and inertia J (Fig. 2A). Each joint is assumed to be independently actuated. All quantities are taken in reference to an inertial frame.

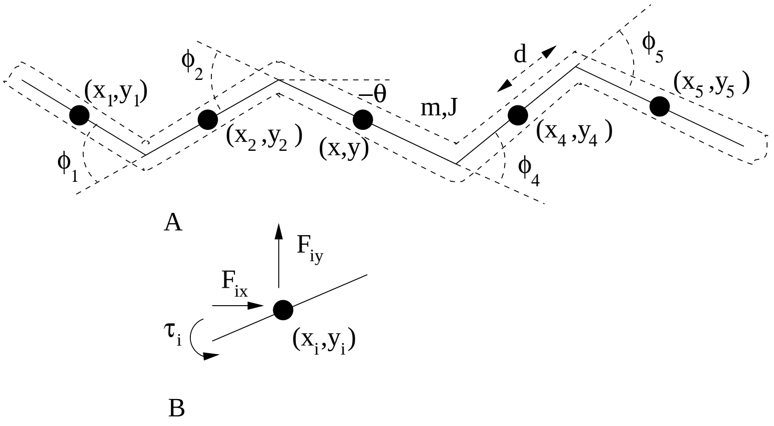

Figure 2: A. Model of the eel as a planar, serial chain of links. B. Forces and torques on link i.

The configuration space is thus $Q = SE(2) \times \mathbb{S}^1 \times \mathbb{S}^1 \times \mathbb{S}^1 \times \mathbb{S}^1$. The variables $(x, y, \theta) \in SE(2)$ describe the position and orientation of the middle link, whereas the joint angles $(\phi_1, \phi_2, \phi_4, \phi_5)$ stand for the shape variables. The Lagrangian of the system is the kinetic energy

$$L = \frac{1}{2}m(\dot{x}^2 + \dot{y}^2) + \frac{1}{2}J\dot{\theta}^2 + \frac{1}{2}J\sum_{i\neq 3}\left(\sum_{j=h(i)}^{i}\dot{\phi}_j + \dot{\theta}\right)^2 + \frac{1}{2}m\sum_{i\neq 3}\left(\dot{x}_i^2 + \dot{y}_i^2\right) ,$$

where (x_i, y_i) is a short-hand notation to denote

$$\begin{pmatrix} x_i \\ y_i \end{pmatrix} = \begin{pmatrix} x \\ y \end{pmatrix} + sg(i)d\begin{pmatrix} \cos\theta \\ \sin\theta \end{pmatrix} + sg(i)d\sum_{k=h(i)}^{i} f(i,k)\begin{pmatrix} \cos(\theta + \sum_{j=h(i)}^{k}\phi_j) \\ \sin(\theta + \sum_{j=h(i)}^{k}\phi_j) \end{pmatrix} .$$

The functions sg, f, and h are given by

$$sg(i) = \begin{cases} -1 & \text{if } i < 3 \\ 1 & \text{if } i > 3 \end{cases} \qquad f(i,k) = \begin{cases} 2 & \text{if } i \neq k \\ 1 & \text{if } i = k \end{cases} \qquad h(i) = \begin{cases} 2 & \text{if } i < 3 \\ 4 & \text{if } i > 3 \end{cases}$$

In fact, (x_i, y_i) corresponds to the coordinates of the center of the i^{th} link[1]. A straightforward computation shows that L is $SE(2)$-invariant. Before writing the expression for the reduced Lagrangian ℓ, we introduce a scaling to nondimensionalize the variables. Let

$$\bar{x} = \frac{x}{d}\,,\ \bar{y} = \frac{y}{d}\,,\ \bar{\theta} = \theta\,,\ \bar{p} = \frac{p}{md}\,,\ \bar{\phi}_i = \phi_i\,,\ \bar{J} = \frac{J}{md^2}\,. \tag{11}$$

---

[1] We remark that although the formulae are written explicitly for the 5-link case, the equations are easily generalized to an n-link robot (n odd), with θ measured at the center link.

Then we have that

$$\ell = \frac{1}{2}(\xi^T, \dot{r}^T)\begin{pmatrix} I(r) & I(r)\mathsf{A}(r) \\ \mathsf{A}^T(r)I(r) & m(r) \end{pmatrix}\begin{pmatrix} \xi \\ \dot{r} \end{pmatrix},$$

where

$$I = \begin{pmatrix} 5 & 0 & 3(s_2 - s_4) + s_{12} - s_{45} \\ 0 & 5 & 3(c_4 - c_2) + c_{45} - c_{12} \\ 3(s_2 - s_4) + s_{12} - s_{45} & 3(c_4 - c_2) + c_{45} - c_{12} & I_{33} \end{pmatrix},$$

$$I\mathsf{A} = \begin{pmatrix} s_{12} & s_{12} + 3s_2 & -(s_{45} + 3s_4) & -s_{45} \\ -c_{12} & -(c_{12} + 3c_2) & c_{45} + 3c_4 & c_{45} \\ 1 + 2c_1 + c_{12} + \bar{J} & (I\mathsf{A})_{32} & (I\mathsf{A})_{33} & 1 + 2c_5 + c_{45} + \bar{J} \end{pmatrix},$$

$$m = \begin{pmatrix} 1 + \bar{J} & 1 + \bar{J} + 2c_1 & 0 & 0 \\ 1 + \bar{J} + 2c_1 & 6 + 2\bar{J} + 4c_1 & 0 & 0 \\ 0 & 0 & 6 + 2\bar{J} + 4c_5 & 1 + \bar{J} + 2c_5 \\ 0 & 0 & 1 + \bar{J} + 2c_5 & 1 + \bar{J} \end{pmatrix}.$$

and $I_{33} = 4c_1 + 6c_2 + 2c_{12} + 4c_5 + 6c_4 + 2c_{45} + 16 + 5\bar{J}$, $(I\mathsf{A})_{32} = 6 + 4c_1 + 3c_2 + c_{12} + 2\bar{J}$, $(I\mathsf{A})_{33} = 6 + 4c_5 + 3c_4 + c_{45} + 2\bar{J}$. The notation $c_i = \cos\bar{\phi}_i$, $s_i = \sin\bar{\phi}_i$, $c_{ij} = \cos(\bar{\phi}_i + \bar{\phi}_j)$ and $s_{ij} = \sin(\bar{\phi}_i + \bar{\phi}_j)$ is understood. Eq. 5 then reads as

$$\xi = g^{-1}\dot{g} = -\mathsf{A}(r)\dot{r} + I^{-1}(r)p\,.$$

For the modeling of the frictional forces acting on each link (see Fig. 2B), we assume that pressure differentials in the directions parallel to the moving body are decoupled from pressure differentials perpendicular to the body. For the fluid drag model, this yields forces acting at each point on the body as

$$F_i^{\|} = -\mu_w^{\|}\operatorname{sgn}(v_i^{\|}) \cdot (v_i^{\|})^2\,, \quad F_i^{\perp} = -\mu_w^{\perp}\operatorname{sgn}(v_i^{\perp}) \cdot (v_i^{\perp})^2\,, \tag{12}$$

where $\mu_w^{\|}$ and $\mu_w^{\perp}$ are drag coefficients for the water depending on the effective area of the link, its shape and the density of the water, and $v_i^{\|}$, $v_i^{\perp}$ are the projections of the vector $(\dot{x}_i, \dot{y}_i)$ along the direction parallel and perpendicular to the link, respectively. The discontinuity in $\operatorname{sgn}(v)$ implies that this expression is not very tractable for use in calculations. For the purposes of simulation, we limit our attention to a linear, viscous force approximation. This can be thought of as a first-order approximation to the quadratic drag forces described in Eq. 12, which we note are also odd functions of the velocity. In general, for systems with periodic behavior, viscous forces approximations can be used, provided coefficients of friction are chosen to dissipate an equal amount of energy over one cycle of motion [17].

Using this approximation, we have a linear expression for the friction forces of the form $F_{approx}^{\|} = -\mu^{\|}v^{\|}$, $F_{approx}^{\perp} = -\mu^{\perp}v^{\perp}$, where $\mu^{\|}$ and $\mu^{\perp}$ are defined by a least squares fit of Eq. 12 over some small range around $v = 0$. For the viscous friction model, we assume that a force exists developing frictional forces proportional to the parallel and perpendicular velocities of link i as:

$$F_i^{\|} = -\mu_v^{\|} v_i^{\|} \,, \quad F_i^{\perp} = -\mu_v^{\perp} v_i^{\perp} \,, \tag{13}$$

where $\mu_v^{\|}$, $\mu_v^{\perp}$ are coefficients of viscous drag.

With this in mind, the derivation of the expression for the frictional forces for the eel is straightforward, though not trivial, and requires some care in tracking the appropriate transformations. One can find that

$$\tau^{\|} = -\nu C H^T H \begin{pmatrix} \bar{g}^{-1}\dot{\bar{g}} \\ \dot{\phi}_1 \\ \dot{\phi}_2 \\ \dot{\phi}_4 \\ \dot{\phi}_5 \end{pmatrix} \,, \quad \tau^{\perp} = -\lambda C G^T G \begin{pmatrix} \bar{g}^{-1}\dot{\bar{g}} \\ \dot{\phi}_1 \\ \dot{\phi}_2 \\ \dot{\phi}_4 \\ \dot{\phi}_5 \end{pmatrix} \,,$$

with $\bar{\mu}^{\|} = \mu^{\|}/m$, $\bar{\mu}^{\perp} = \mu^{\perp}/m$,

$$C = \begin{pmatrix} 1 & 0 & 0 & 0 & 0 & 0 & 0 \\ 0 & 1 & 0 & 0 & 0 & 0 & 0 \\ 0 & 0 & 1 & 0 & 0 & 0 & 0 \end{pmatrix} \,,$$

$$H = \begin{pmatrix} c_{12} & s_{12} & -(2s_1 + s_{12}) & 0 & -2s_1 & 0 & 0 \\ c_2 & s_2 & -s_2 & 0 & 0 & 0 & 0 \\ 1 & 0 & 0 & 0 & 0 & 0 & 0 \\ c_4 & s_4 & s_4 & 0 & 0 & 0 & 0 \\ c_{45} & s_{45} & 2s_5 + s_{45} & 0 & 0 & 2s_5 & 0 \end{pmatrix} \,, \quad \text{and}$$

$$G = \begin{pmatrix} -s_{12} & c_{12} & -(1 + 2c_1 + c_{12}) & -1 & -(1 + 2c_1) & 0 & 0 \\ -s_2 & c_2 & -(1 + c_2) & 0 & -1 & 0 & 0 \\ 0 & 1 & 0 & 0 & 0 & 0 & 0 \\ -s_4 & c_4 & 1 + c_4 & 0 & 0 & 1 & 0 \\ -s_{45} & c_{45} & 1 + 2c_5 + c_{45} & 0 & 0 & 1 + 2c_5 & 1 \end{pmatrix} .$$

Then, the equation for the momentum, Eq. 6, takes the form

$$\begin{pmatrix} \dot{p}_1 \\ \dot{p}_2 \\ \dot{p}_3 \end{pmatrix} = \begin{pmatrix} \xi_3 p_2 \\ -\xi_3 p_1 \\ \xi_2 p_1 - \xi_1 p_2 \end{pmatrix} + \tau^{\|} + \tau^{\perp} \,.$$

In order to obtain a numerical solution for the path of the eel as a function of time, we will assume that we have full control of the shape variables ϕ_i, $i \neq 3$, that is, $u_i = \dot{\phi}_i$. The assumption of full control of the shape is reasonable since the REEL II has actuators at each joint. A typical example of the motion of the eel can be seen in Fig. 3.

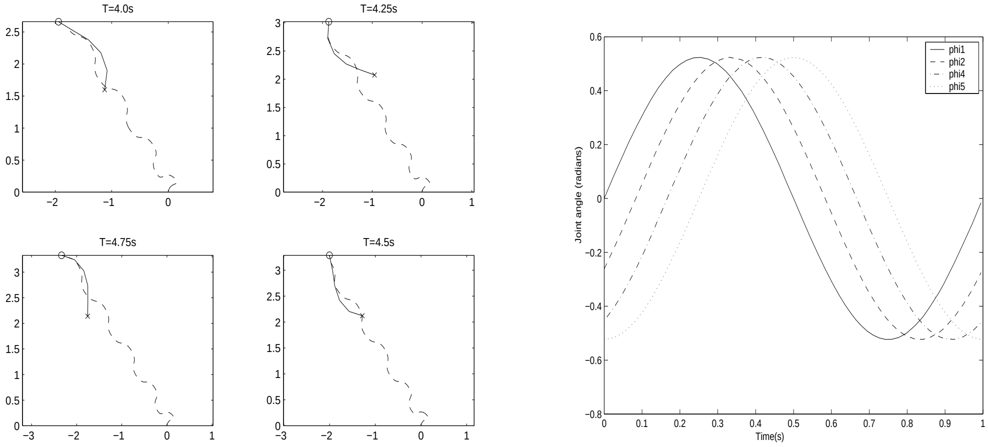

Figure 3: An illustration of the motion of the eel during the forward gait obtained in [39] using traveling waves. The path followed by the robot in the (x, y)-plane is given by the dashed curve in the figure on the left. Several snapshots of the eel's shape are superimposed on the path at times 4.0, 4.25, 4.5 and 4.75. A plot of one cycle of the joint angles is given in the figure on the right.

3 A common setting for Robotic Locomotion

Given the discussion of the previous section, we can consider the following set of equations as an equally valid description of the dynamics of the two classes of locomotion systems we are treating:

$$g^{-1}\dot{g} = -\mathbb{A}(r)\dot{r} + \mathbb{I}^{-1}(r)p\,, \tag{14}$$

$$\dot{p} = \frac{1}{2}\dot{r}^T\sigma_{\dot{r}\dot{r}}(r)\dot{r} + p^T\sigma_{p\dot{r}}(r)\dot{r} + \frac{1}{2}p^T\sigma_{pp}(r)p + \rho_{\dot{r}}(r)\dot{r} + \rho_p(r)p\,, \tag{15}$$

$$\ddot{r} = w\,. \tag{16}$$

Observe that Eq. 15 includes the full set of terms to take into account the presence of both nonholonomic constraints and linear forcing functions. Note also that, since we assume full control of the shape variables, we have recast to our convenience Eq. 7 (respectively, Eq. 10) as Eq. 16.

These equations can be put into the standard form of a nonlinear control system with affine inputs. If the matrix $\sigma_{\dot{r}\dot{r}} \equiv 0$ (as is the case for the eel), we take as states $z = (g, p, r) \in G \times \mathbb{R}^s \times M$, where s denotes the dimension of the unconstrained fiber directions (which coincides with $k = \dim G$ for anguilliform locomotion). Define the nonzero drift term

$$f(z) = \begin{pmatrix} g\,\mathbb{I}^{-1}(r)p \\ \frac{1}{2}p^T\sigma_{pp}(r)p + \rho_p(r)p \\ 0 \end{pmatrix} \,,$$

and consider the vectors

$$B_i(z) = \begin{pmatrix} -g\mathbb{A}(r)e_i \\ (p^T\sigma_{p\dot{r}}(r) + \rho_{\dot{r}}(r))e_i \\ e_i \end{pmatrix} \,, \quad 1 \le i \le \dim(M) = m \,,$$

where e_i is an m-vector having a 1 in the i^{th} row and 0 otherwise. Putting $B = (B_i(z))$, we can rewrite Eqs. 14–16 as

$$\dot{z}(t) = f(z) + B(z)u \,, \tag{17}$$

where $u(t) \in \mathbb{R}^m$ is considered to be the input vector, defined by $u_i(t) = \bar{w}_i(t)$, with $\bar{w}_i(t) \equiv \int_0^t w_i(s)ds$, i.e. u is a velocity. In the case that $\sigma_{\dot{r}\dot{r}}(r) \not\equiv 0$ (as is the case, for example, with the snakeboard), we must use the full, dynamically extended system, so that the state variable is now $z = (g, p, r, \dot{r}) \in G \times \mathbb{R}^s \times TM$, the input is $u = w$ (that is, an acceleration), and the quantities in Eq. 17 are redefined as

$$f(z) = \begin{pmatrix} -g\mathbb{A}(r)\dot{r} + g\mathbb{I}^{-1}(r)p \\ \frac{1}{2}\dot{r}^T\sigma_{\dot{r}\dot{r}}(r)\dot{r} + p^T\sigma_{p\dot{r}}(r)\dot{r} + \frac{1}{2}p^T\sigma_{pp}(r)p + \rho_{\dot{r}}(r)\dot{r} + \rho_p(r)p \\ \dot{r} \\ 0 \end{pmatrix} ,$$

$$B_i(z) = \begin{pmatrix} 0 \\ 0 \\ 0 \\ e_i \end{pmatrix} , \quad 1 \le i \le \dim(M) = m \,.$$

In the following, we will denote by d the dimension of the state space, which will correspond to either $d = n + s$ or $d = n + s + m$, depending on the case considered.

Let us assume that the system described by Eqs. 14–16 is controllable. This means that given initial and final states, z_0 and z_f, with z_f sufficiently close to z_0, there exists a control input $u^*(t)$ such that the solution $z^*(t)$ of Eq. 17 with $z^*(0) = z_0$ satisfies $z^*(T) = z_f$. The examples of the snakeboard and the robotic eel are both controllable systems [39, 48]. For general systems of the form given by Eq. 17, there exist some computable criteria to verify this property developed elsewhere [53], and further refined for nonholonomically constrained systems with symmetry in [48].

4 The optimal control problem: The Basis Algorithm

Having established Eqs. 14–16 as a common setting for nonholonomically constrained and anguilliform locomotion, we are next interested in determining what the best set of inputs is to generate a given motion. For instance, for the eel this would imply effecting the desired motion without spending "too much" energy. Since our main concern is to obtain ***gaits*** or cyclic paths in the shape variables resulting in a net motion of the system, we will restrict our attention to the following class of input functions

$$\mathcal{U} = \{u : [0,T] \longrightarrow \mathbb{R}^m \mid u(t) \,\text{is piecewise differentiable and}\, u(0) = u(T)\}\ .$$

Then, we would like to find the solution to the following Optimal Control Problem (OCP).

OCP1: *Let z_0, z_f be initial and final states. Determine the control inputs $u \in \mathcal{U}$ steering the system defined in Eq. 17 from z_0 to z_f after time $T > 0$ while minimizing the cost functional*

$$\mathcal{J}(u) = \int_0^T \left(u_1(t)^2 + \cdots + u_m(t)^2\right) dt = \int_0^T \langle u\,, u\rangle dt\,.$$

Note that u is regarded as a function in $L_2([0,T];\mathbb{R}^m) \equiv L_2([0,T])$ with associated norm $\|u\|_2^2 \triangleq \mathcal{J}(u)$.

In answering a similar question for driftless control systems, in [21, 22] it was observed that, because of the form of the functional $\mathcal{J}$, the OCP1 can be reformulated as an infinite dimensional problem in l_2. In fact, let $\{\mathbf{e}_i(t)\}_{i=1}^{\infty}$ be an orthonormal basis for $L_2[0,T]$. Then, the inputs $u(t)$ can be expressed as $u(t) = \sum_{i=1}^{\infty} \alpha_i \mathbf{e}_i(t)$ for some sequence $\alpha = (\alpha_i)_{i=1}^{\infty} \in l_2$ and the OCP1 can be rephrased as follows,

OCP2: *Given initial and final states, z_0 and z_f, and the equations*

$$\dot{z} = f(z) + B(z)u\,,\ \ u(t) = \sum_{i=1}^{\infty} \alpha_i \mathbf{e}_i(t)\,, \tag{18}$$

find $\alpha \in l_2$ of minimum cost, $\mathcal{J}(\alpha) = \sum_{i=1}^{\infty} \alpha_i^2 \triangleq \|\alpha\|_{l_2}^2$, such that the solution of Eq. 18 starting from z_0 reaches z_f at time $t = T$.

Obviously, finding one exact solution of this infinite dimensional problem, if such a solution exists, would imply great computational difficulties. However, following the idea of Ritz Approximation Theory, one can alternatively try to approximate the solutions of the finite dimensional problems that arise from the truncation of Eq. 18 to the first N basis elements. That is, for $N > 0$ we restrict the set of inputs to

$$\mathcal{U}_N = \left\{ u \in \mathcal{U} \mid u(t) = \sum_{i=1}^{N} \alpha_i \mathbf{e}_i(t)\,, \alpha = (\alpha_1, \ldots, \alpha_N) \in \mathbb{R}^N \right\}\ .$$

Due to the nature of undulatory locomotion systems, the method proposed in [22] with the basis induced by $\{\sin nt, \cos nt\}_{n=1}^{\infty}$ is very appropriate for treating these systems with nonzero drift. In this way, we focus on a subclass of periodic inputs and look for suboptimal solutions producing ***near-optimal*** gaits. Furthermore, the examples we have tested so far show precisely that the modes playing the most important roles are those corresponding to low frequencies, so it is not unreasonable at all to restrict the controls to the first basis elements. The general issue of whether the system is still controllable using this truncated basis is a subtle one. However, it has been shown that undulatory locomotion systems, such as the snakeboard [36, 45], are locally controllable using such a class of inputs. We are also confident, based on series expansions for several classes of nonlinear control systems, that the same can be said for most controllable systems given a sufficient number of input basis elements.

In the sequel, we briefly discuss the *Basis Algorithm* developed in [21, 22] and its adaptation for control equations with nonzero drift. For the technical details of the algorithm we refer the reader to the cited articles.

4.1 Basis Algorithm

Let N be a nonzero integer and define the $m \times N$ matrix $\Phi = (\mathbf{e}_1, \ldots, \mathbf{e}_N)$. Truncating Eq. 18 to the first N basis elements we get

$$\left\{ \begin{array}{l} \dot{z} = f(z) + B(z)\, \Phi\, \alpha^T \\ z(0) = z_0\,. \end{array} \right. \tag{19}$$

A given input $u \in \mathcal{U}_N$, or equivalently $\alpha = (\alpha_1, \ldots, \alpha_N) \in \mathbb{R}^N$, determines a solution $z(t, \alpha)$ of Eq. 19. Clearly, since $f(z)$ and $B(z)$ are differentiable, the terminal point of this solution $z(T, \alpha)$ will vary smoothly with α. Define then the function $g : \mathbb{R}^N \longrightarrow \mathbb{R}^d$ by $g(\alpha) = z(T, \alpha)$ and let z_f be the final state where we want to steer the system. Let $\|\cdot\|_{\mathbb{R}^d}$ denote the Euclidean norm of $\mathbb{R}^d$. Now, we approximate the original OCP2 in l_2 by the finite-dimensional problem $P_{N,\gamma}$ in $\mathbb{R}^N$ defined as follows:

$P_{N,\gamma}$: *Given $N \in \mathbb{N}$ and $\gamma > 0$, determine the solutions $(z^*_{N,\gamma}, \alpha^*_{N,\gamma})$ of Eq. 19 that minimize*

$$\mathcal{J}_{N,\gamma}(\alpha) = \langle \alpha, \alpha \rangle + \gamma \|g(\alpha) - z_f\|^2_{\mathbb{R}^d} \triangleq \sum_{i=1}^{N} \alpha_i^2 + \gamma \|g(\alpha) - z_f\|^2_{\mathbb{R}^d}\,.$$

Note that $g(\alpha^*_{N,\gamma}) = z^*_{N,\gamma}(T)$.

In the following, we describe a procedure to numerically approximate the solutions of $P_{N,\gamma}$. Put $\sigma = \dfrac{1}{\gamma}$ and alternatively consider

$$\mathcal{J}_{N,\sigma}(\alpha) = \sigma \langle \alpha, \alpha \rangle + \|g(\alpha) - z_f\|^2_{\mathbb{R}^d}\,.$$

Assume that α_k is an approximation of $\alpha^*_{N,\sigma}$, the global minimum of $\mathcal{J}_{N,\sigma}$. If $g(\alpha)$ is known, we can utilize ideas from quadratic programming to find a modified Newton's rule, given by

$$\alpha_{k+1} = \alpha_k - \mu(\sigma I + A^T A)^{-1}(\sigma\alpha_k + A^T(g(\alpha_k) - z_f))\,, \tag{20}$$

to update α_k. Here, I denotes the identity matrix, $A = \dfrac{\partial g}{\partial \alpha}(\alpha_k)$ and $0 < \mu < 1$ is a parameter. In order to save computational time, the inverse of the positive definite matrix $I + A^T A$ can be replaced by the inverse of $A^T A$ when $\sigma \ll 1$. We may also vary μ, increasing its value from 0 to 1 as α_k reaches $\alpha^*_{N,\sigma}$, to speed up the convergence of the algorithm.

Since g is smooth, it can be shown that there exists a σ_0 such that $\forall 0 < \sigma \leq \sigma_0$, $\mathcal{J}_{N,\sigma}(\alpha)$ is locally convex near a solution of our truncated problem. Thus, we can guarantee the convergence of the sequence $\{\alpha_k\}$ to $\alpha^*_{N,\sigma}$ whenever we start from a close enough α_0 and σ is small enough. Accordingly, we always took a very small σ in our simulations. We first looked for a α_0 approximately steering the system from z_0 to z_f based on the perturbation analysis described in [38, 39] and ran the algorithm to obtain a solution α. We checked that running the algorithm with several different initial conditions α_0 we obtained the same optimal solution. That led us to reasonably assume that the algorithm was not giving a local minima, but the true optimal solution. Of course, a more thorough analysis on the region of convergence of the algorithm would be necessary, but will not be treated here.

In order to implement the method we need to compute $g(\alpha_k)$ and its Jacobian A. If $g(\alpha)$ is not known, the following numerical method can be used. Consider the function $Y(t) = \dfrac{\partial z}{\partial \alpha}(t)$. It is clear that $Y(T) = A$. Note also that $Y(0) = \lim_{t\to 0} Y(t) = 0$. A differential equation for $Y(t)$, obtained from Eq. 19, is given by

$$\begin{aligned}\dot{Y}(t) &= \frac{d}{dt}\frac{\partial z}{\partial \alpha} = \frac{\partial \dot{z}}{\partial \alpha} = \frac{\partial}{\partial \alpha}\left(f(z) + B(z)\Phi\,\alpha^T\right)\\ &= \frac{\partial f}{\partial z}\frac{\partial z}{\partial \alpha} + \sum_{i=1}^{m}\frac{\partial B_i}{\partial \alpha}u_i + B\Phi = \left(\frac{\partial f}{\partial z} + \sum_{i=1}^{m}\frac{\partial B_i}{\partial z}u_i\right)Y + B\Phi\,.\end{aligned}$$

Thus, in order to update α_k, the following differential equations must be integrated from 0 to T,

$$\left\{\begin{aligned} &\dot{z} = f(z) + B(z)\,\Phi\,\alpha_k^T\,, \quad z(0) = z_0\,,\\ &\dot{Y} = \left(\frac{\partial f}{\partial z} + \sum_{i=1}^{m}\frac{\partial B_i}{\partial z}u_i\right)Y + B\Phi\,, \quad Y(0) = 0\,,\end{aligned}\right. \tag{21}$$

so we can set $g(\alpha_k) = z(T)$ and $A = Y(T)$.

We have summarized this procedure in terms of the algorithm described in Table 1.

Input:

Initial and final states z_0, $z_f \in \mathbb{R}^d$.
Vector fields $f(z)$ and $B_i(z)$, $1 \leq i \leq m$.

Step 0:

(i) Choose $N > 0$ and define $\Phi = (\mathbf{e}_1, \ldots, \mathbf{e}_N)$.
(ii) Initialize with $\alpha \equiv \alpha_0$.

Step 1:

(i) Choose $0 < \gamma$ and $0 < \mu < 1$.

Step 2:

(i) Solve the set of differential equations given by Eq. 21.
(ii) Set $g(\alpha) = z(T)$ and $A = Y(T)$.
(iii) Update α according to the modified Newton's rule (cf. Eq. 20).

Step 3:

(i) Examine $\|g(\alpha) - z_f\|_{\mathbb{R}^d}$ and $|\mathcal{J}_{N,\gamma}(\alpha_{updt}) - \mathcal{J}_{N,\gamma}(\alpha)|$.
(ii) If the results are satisfactory enough, exit. Else if they verify a certain tolerance dependent on γ and μ, go to Step 1, increasing the value of γ and/or μ. Otherwise, repeat Step 2.

Output:

Approximation to the optimal control input $u(t)$, $t \in [0, T]$, linking z_0 and z_f.

Table 1: Basis Algorithm

Remark 4.1. Note that for driftless control equations it is necessary to choose $\alpha_0 \neq 0$ to initiate the algorithm, but this is not the case when z_0 is not an equilibrium point of the nonzero drift vector field f. In our simulations for the eel, we made use of the perturbation analysis described in [38, 39] to choose α_0 with a few nonzero entries to let the algorithm develop smoothly by itself the coefficients of the optimal solution α_N^*.

Remark 4.2. When running the Basis Algorithm, it is convenient to increase γ and μ from smaller to bigger values as α comes close to the solution (which is determined by the desired configuration z_f and the actual one $z(T)$, and the fact that the cost ceases to decrease). As a result, the robustness and performance of the algorithm are improved. This procedure is based on the observation made in [22] in the sense that when α is far from its solution, by choosing μ small we can always make the cost function decrease. This can easily be extended from driftless systems to the class of systems under consideration.

Remark 4.3. In the computations for our examples, we have always taken $N = 2fm$, where $m = \dim M$ is the number of input functions and f is the maximum frequency we want to consider at each input, which in our simulations was $f \leq 5$. The open-loop control of several undulatory locomotion systems [39, 36, 49] shows that the modes playing the most important roles are those corresponding to low frequencies, so it seems reasonable to restrict the controls to the first basis elements. The addition of higher modes (that is, increasing f) slightly modifies the solution, in accordance with the analysis of Section 4.2, which shows that by increasing N and γ, we get closer to the optimal solution of OCP2. We note, though, that the main role in this optimal solution is still played by the first modes.

We have chosen then the following orthonormal basis of $L_2[0, 2\pi]$,

$$\begin{aligned}
&\mathbf{e}_1 = \frac{1}{\sqrt{\pi}} \sin t \; e_1 \, , \; \mathbf{e}_2 = \frac{1}{\sqrt{\pi}} \cos t \; e_1 \, , \\
&\vdots \\
&\mathbf{e}_{2f-1} = \frac{1}{\sqrt{\pi}} \sin(ft) \; e_1 \, , \; \mathbf{e}_{2f} = \frac{1}{\sqrt{\pi}} \cos(ft) \; e_1 \, , \\
&\vdots \\
&\mathbf{e}_{N-2f+1} = \frac{1}{\sqrt{\pi}} \sin t \; e_m \, , \; \mathbf{e}_{N-2f+2} = \frac{1}{\sqrt{\pi}} \cos t \; e_m \, , \\
&\vdots \\
&\mathbf{e}_{N-1} = \frac{1}{\sqrt{\pi}} \sin(ft) \; e_m \, , \; \mathbf{e}_N = \frac{1}{\sqrt{\pi}} \cos(ft) \; e_m \, ,
\end{aligned}$$

where recall that e_i, $1 \leq i \leq m$ denotes the standard i^{th} basis element, as defined above.

4.2 Correctness of the Basis Algorithm

As was mentioned earlier, the idea underlying the method is that by making γ and N tend to infinity, we will obtain solutions $(z_{N,\gamma}, u_{N,\gamma})$ of $P_{N,\gamma}$ which tend to solutions (z_*, u_*) of the original problem. In fact, the type of convergence found in [21, 22] for driftless systems can be readily extended to systems with nonzero drift that are bounded input, bounded state (BIBS) stable. That is,

Assumption 1. There exists a continuous function $\phi(\delta, z_0)$, $\delta \geq 0$ *such that if* $\|u\|_2 \leq \delta$ *then the corresponding solution* $z(t)$ *of Eq. 17 verifies* $\|z\|_{C[0,T]} = sup_{t\in[0,T]}\|z(t)\|_{\mathbb{R}^d} \leq \phi(\delta) < \infty$.

Under this assumption, we have the following result.

Theorem 4.4. *Let* $S_* \subseteq C[0,T] \oplus L_2[0,T]$ *be the set of optimal solutions* (z_*, u_*) *of the original system OCP2 with optimal cost* $\mathcal{J}_*$, *and let* $S_{N,\gamma} \subset C[0,T] \oplus L_2[0,T]$ *be the set of optimal solutions* $(z_{N,\gamma}, u_{N,\gamma})$ *of the approximated problem* $P_{N,\gamma}$ *with optimal cost* $\mathcal{J}_{N,\gamma}$. *Then,* $\{S_{N,\gamma}\}$ *converge to* S_* *in the sense*

$$\lim_{\gamma\to\infty} \lim_{N\to\infty} d(S_{N,\gamma}, S_*) = 0\,,$$

and $\{\mathcal{J}_{N,\gamma}\}$ *converges to* $\mathcal{J}_*$ *in the sense*

$$\lim_{\gamma\to\infty} \lim_{N\to\infty} \mathcal{J}_{N,\gamma} = \mathcal{J}_*\,.$$

Here, the measure d *of* $C[0,T] \oplus L_2[0,T]$ *is defined as*

$$d(X, Y) = \sup_{\{(z,u)\in X\}} \inf_{\{(\bar{z},\bar{u})\in Y\}} \left(\|z - \bar{z}\|_{C[0,T]} + \|u - \bar{u}\|_2\right)\,,$$

for X, $Y \subset C[0,T] \oplus L_2[0,T]$.

The proof of Theorem 4.4 for systems with nonzero drift is similar to that of the driftless case developed in [21], taking into account the next two simple lemmas:

Lemma 4.5. *Let* $\{u_k\}_{k=1}^{\infty}$ *be a sequence of inputs in* $L_2[0,T]$ *such that* $\|u_k - u\|_2 \to 0$, *for some* $u \in L_2[0,T]$, *and let* $\{z_k\}$, z *be the corresponding solutions of Eq. 17, respectively. Then, for a fixed* $\gamma > 0$, *there exists* $k_0 > 0$ *such that for all* $k \geq k_0$,

$$\|z_k\|_{C[0,T]} < \gamma + \phi(\delta)\,, \;\; \textit{if} \quad \|u\|_2 < \delta\,.$$

Lemma 4.6. *Let* $\{u_k\}_{k=1}^{\infty}$ *be a sequence of inputs in* $L_2[0,T]$ *such that* $\|u_k - u\|_2 \to 0$, *for some* $u \in L_2[0,T]$, *and let* $\{z_k\}$, z *be the corresponding solutions of Eq. 17, respectively. Assume that both* f *and* B *are at least* C^1. *Then, for all* $\gamma_0 > 0$, *there exists* $k_0 > 0$ *such that for all* $k \geq k_0$,

$$\|z_k - z\|_{C[0,T]} \leq L\|u_k - u\|_2\,, \;\; \textit{if} \quad \|u\|_2 < \delta\,,$$

where L *is a constant depending on* γ_0 *and* $\|u\|_2$.

We refer to the appendix for the proof of these results.

Remark 4.7. In other words, Theorem 4.4 ensures that given a sequence of solutions $\left\{(z_{N,\gamma_p}, u_{N,\gamma_p}) \in S_{N,\gamma_p}\right\}$ there exists a subsequence $\{(z_{N_k,\gamma_{p_l}}, u_{N_k,\gamma_{p_l}})\}_{k,l=1}^{\infty}$ and a solution $(z_*, u_*) \in S_*$ such that

$$\begin{aligned} \|u_{N_k,\gamma_{p_l}} - u_*\|_2 &\longrightarrow 0 \\ \|z_{N_k,\gamma_{p_l}} - z_*\|_{C[0,T]} &\longrightarrow 0\,, \end{aligned}$$

as N_k, γ_{p_l} tend to infinity.

Remark 4.8. For the example of the eel, taking into account that the friction term $\rho_p(r)p + \rho_{\dot r}(r)\dot r$ always opposes its motion, we can consider that the physical solutions $(z(t), u(t))$ are such that $\|p(t)\| \leq C < \infty$, for sufficiently large $C \gg 0$. With this hypothesis on the solutions one can easily prove BIBS stability.

5 Simulations for the eel

In all the simulations shown below, we have used the nondimensional equations describing the motion of the robotic eel. Thus, the axes on the plots are all unitless. The friction coefficients $\bar\mu^{\perp}$ and $\bar\mu^{\parallel}$ are set to 18 and 1.8, respectively. The non-dimensional inertial parameter $\bar J$ is taken to be 0.37. These values are taken to match experimental data taken in previous work [41]. The cost to optimize is then

$$\mathcal{J} = \int_0^T \left(\dot\phi_1^2 + \dot\phi_2^2 + \dot\phi_4^2 + \dot\phi_5^2\right) dt\,,$$

which corresponds to the energy expenditure of the joint actuators. The final time is $T = 2\pi$, and the initial and final values of the orientation angle θ and of the joint angles are set to zero, except when making comparisons with the traveling wave simulations and where otherwise specified. Also, the maximum frequency considered is always $f = 5$ in each input function.

5.1 Forward motion

In this section, we present three different optimal gaits for the eel, all of them having in common a forward displacement.

Forward motion with zero initial and final momentum

We first ran the Basis Algorithm setting $(x_0, y_0) = (0, 0)$ and $(x_f, y_f) = (3, 0)$. The optimal motion of the eel can be observed in Fig. 4. Roughly speaking, it seems that the eel tries to execute a traveling wave, adjusting at the same time the initial and final configurations that we have specified.

More precisely, it can be observed in the figure that the eel starts from a straight position and quickly evolves to the first peak in the (x, y)-plot, where the links acquire a shape ready for a traveling wave. This leads to a sort of "bursting" behavior – the eel first coils up in the proper way and then springs forward in a way that generates the most momentum gain possible. During this bursting period, the eel moves through to the largest value in y, creating at the same time the largest value of the p_1 component of the momentum. The traveling wave continues further in time, until in the last part of this cycle the eel adjusts itself to the final state, while at the same time allowing the friction forces to dissipate the momentum down to its final value.

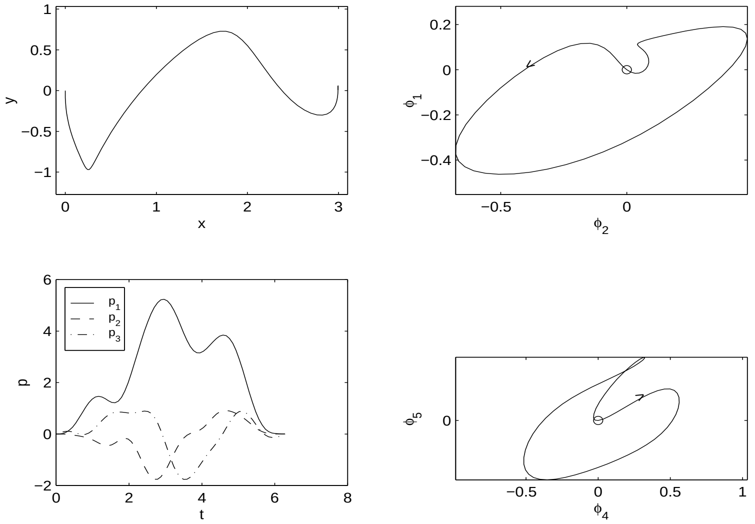

Figure 4: Forward motion of the eel, with zero initial and final momentum. The initial and final points for the shape trajectories are marked with a "o" and the evolution directions are depicted with arrows. The cost is $\mathcal{J} = 4.72435$.

Building up momentum

In this case, we ran the Basis Algorithm setting $(x_0, y_0) = (0, 0)$ and $(x_f, y_f) = (3, 0)$, and the final momentum p_1 was set equal to 2. As a consequence, this gait is similar to the former one, except for the fact that the eel does not let the friction dissipate all its momentum.

Note in Fig. 5 the same coiling behavior at the beginning. After that, the eel smoothly evolves in a kind of traveling wave, with the amplitudes of the angles ϕ_1 and ϕ_5 smaller than the other two. We note that this makes sense since the motion of the two outer

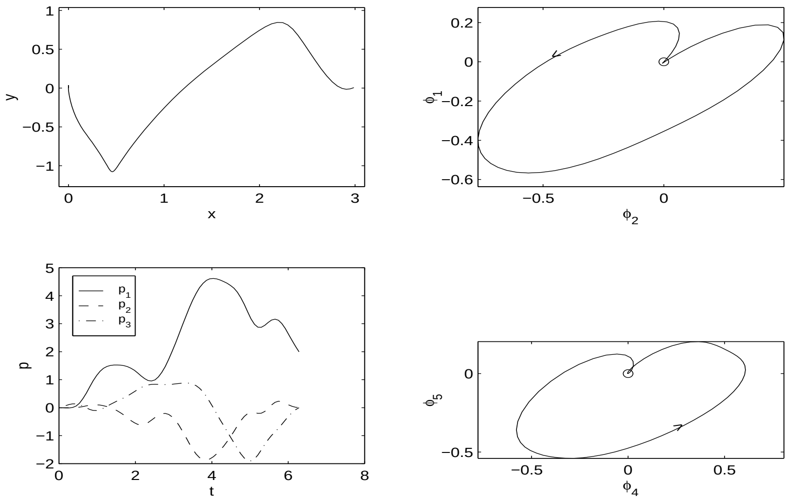

Figure 5: Forward motion of the eel building up momentum. The initial and final points for the shape trajectories are marked with a “o” and the evolution directions are depicted with arrows. The cost is $\mathcal{J} = 4.1058$.

links will generate less propulsive effect than those more central to the body. This is partially seen in biological eels, where the head generally moves less than the rest of the body, though clearly this may be for different reasons than optimization of energy.

The fast transition to the traveling wave in both this gait and the former one can be seen in the joint angle plots of Figs. 4 and 5. The graphs quickly “escape” from the initial and final point $(0, 0)$, to reach the traveling wave.

Traveling wave versus optimal motion

In this simulation, we compare the optimal gaits generated using the Basis Algorithm method with the open-loop gaits proposed in [39], some of which are motivated by biological observations [25]. In this and subsequent comparisons, the initial and final states for the optimal solutions are chosen to match those found in the corresponding traveling wave approach, so that a direct comparison can be made. For this reason, the optimal gaits and the associated costs are different than in the previous cases, where the initial and final states are chosen with a fully extended configuration ($\phi_i = 0$).

The path described in the (x, y)-plane by the eel under both simulations look quite similar (see Fig. 6). The optimal gait in the shape variables seems to be a kind of deformation of the traveling wave, just the one needed to generate almost the same time evolution (just a little larger) in the forward momentum, p_1, and in the components, p_2 and p_3 (just a little smaller).

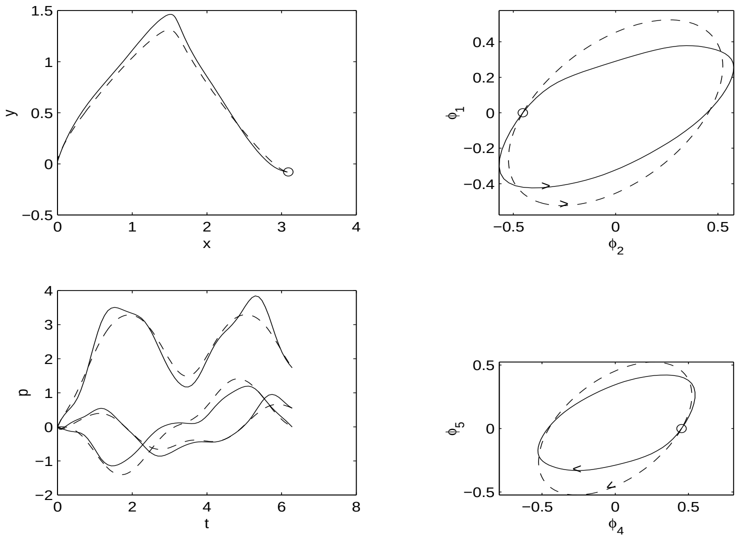

Figure 6: Comparison between a traveling wave (shown dashed) as used in [39] and the optimal approach (shown solid) of the forward motion of the eel building up momentum. The costs are $\mathcal{J} = \pi^3/9 \approx 3.44514$ and $\mathcal{J} = 2.9$, respectively. The initial and final points for the shape trajectories are marked with a "o" and the evolution directions are depicted with arrows.

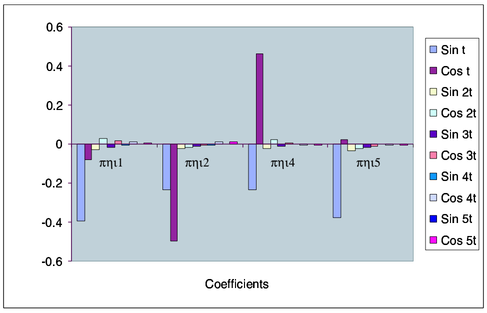

Figure 7: The first five harmonics of the optimal forward motion of Fig. 6.

It is interesting to note that the magnitudes of the joint angles ϕ_1 and ϕ_5 are quite smaller than in the traveling wave, whereas with the other two angles, ϕ_2 and ϕ_4, they are quite similar. Indeed, the optimal gait seems to be a traveling wave with smaller amplitudes in the head and tail of the eel. This is supported by looking at the coefficients for the higher harmonics, as shown in Fig. 7, which are basically negligible in comparison to the fundamental frequency. Also, in relation to the other comparisons presented below, this comparison is the one that presents the smallest saving of energy.

This suggests that the traveling wave approach used in [39] is actually very appropriate to drive the eel.

5.2 Turning motion

In this section we show the comparison of the optimal approach with the traveling wave approach for the rotation gait.

Traveling waves versus optimal motion

As said before, the initial and final states for the optimal solutions are chosen to match those found in the corresponding traveling wave gait. Note that in this comparison the shape plots are quite different between the two gaits (see Fig. 8). The relative saving of energy is also much larger than in the comparison of the forward motion. This gait had very interesting behaviors when tested experimentally, as we will show in Section 5.4.

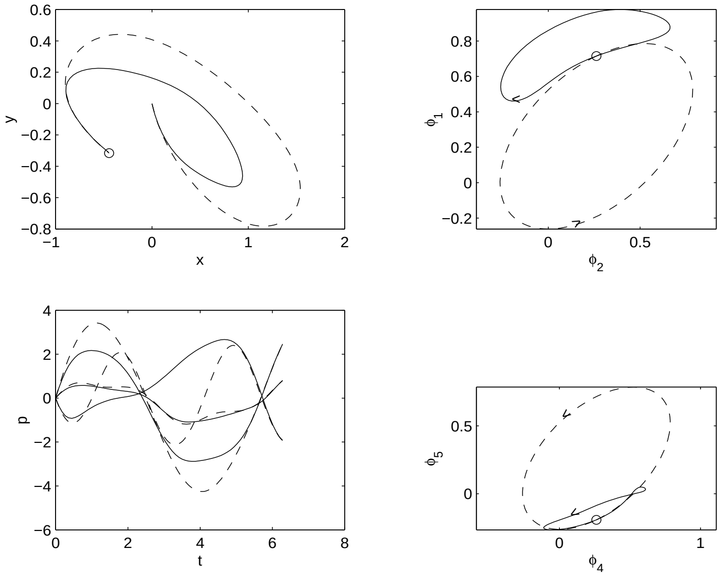

Figure 8: Comparison between the traveling waves (shown dashed) as used in [39] and the optimal approach (shown solid) of the turning in place motion of the eel. The costs are $\mathcal{J} = \pi^3/9 \approx 3.44514$ and $\mathcal{J} = 1.4414$, respectively. The initial and final points for the shape trajectories are marked with a "o" and the evolution directions are depicted with arrows.

5.3 Lateral motion (parallel parking)

In this section, we present two parallel parking gaits (that is, gaits that generate motion in the direction perpendicular to the forward direction pointed by the eel robot). The first one has zero initial and final momentum, whereas the second one is a comparison with the traveling wave approach.

Lateral motion with zero initial and final momentum

In this case, we ran the Basis algorithm with $(x_0, y_0) = (0, 0)$ and $(x_f, y_f) = (0, 2)$. The motion of the eel during the execution of the gait can be observed in Fig. 9. Note that the effect of this gait in the (x, y) plane is similar in nature to that one of the optimal lateral (or parallel parking) gait found in another dynamic robotic locomotion system, the snakeboard system [13, 50]. It is interesting to notice that the maximum values of the forward and lateral momentum occur almost simultaneously and are located in the (x, y) plot around $x = -0.6$.

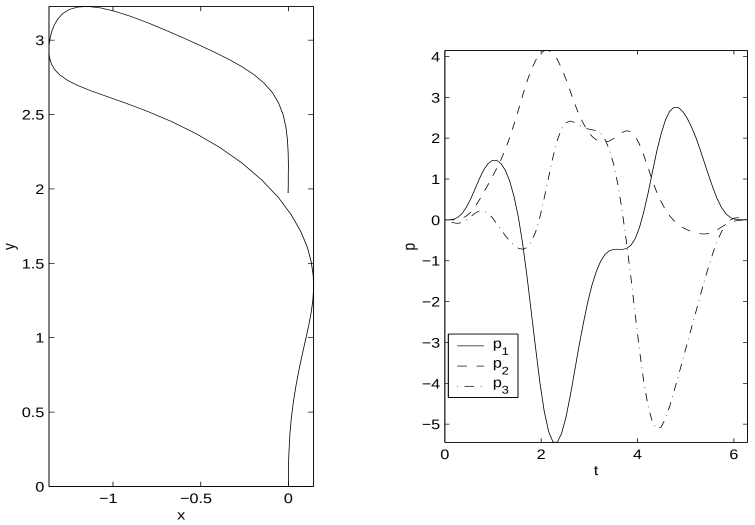

Figure 9: Lateral motion of the eel, with zero final momentum. The cost is $\mathcal{J} = 7.9147$.

Unfortunately, the optimal inputs for the shape angles drive them to values near 180° (there is a significant amount of “coiling”), so it was impossible to test this gait in our real experiments.

Traveling waves versus optimal motion

Note in the comparison with the traveling wave gait that the motion in the variable x is practically unnoticeable (see Fig. 10). As in the turning gait, the shape plots are quite different. Observe also the relative saving of energy.

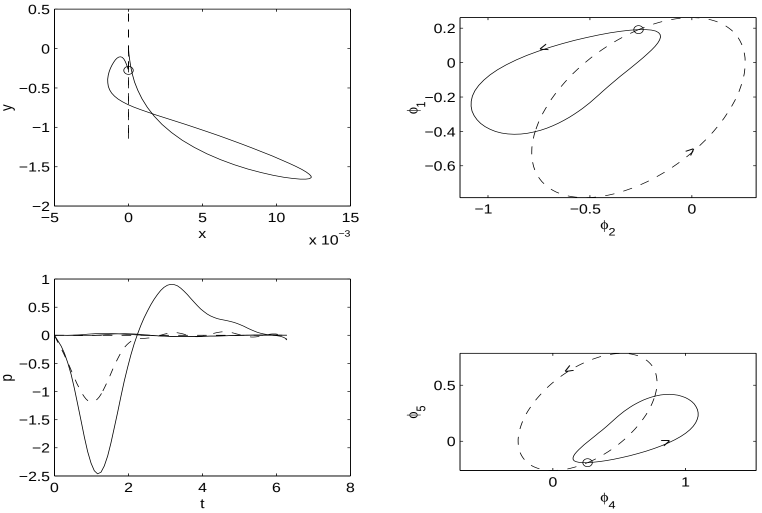

Figure 10: Comparison between the traveling waves as used in [39] and the optimal approach (shown solid) of the sideways motion of the eel. The costs are $\mathcal{J} = \pi^3/9 \approx 3.44514$ and $\mathcal{J} = 2.05$, respectively. The initial and final points for the shape trajectories are marked with a "o" and the evolution directions are depicted with arrows.

The magnitudes of the joint angles ϕ_1 and ϕ_5 in the optimal gait are half the size of those found in the traveling waves, again suggestive of the biological observation that the head (and sometimes the tail) of the eel tend to move less than the rest of the body. We again could not implement this gait in real experiments, due to the limitations on the maximum joint angles for the REEL II robot.

5.4 Comparison with experimental motions

We have implemented in the REEL II robot several optimal gaits. The experimental set-up is the following. The robot shape is radio-controlled. A PC ground station calculates the shape variables (joint angles) corresponding to each of them, which are transmitted using an off-the-shelf radio controller and a custom built, PIC microcontroller-based PC/RC converter to a receiver in the nose of the robot. Using off-the-shelf RC components, control of the robot is possible to depths of approximately 1m, although our system is designed to operate only on the surface. The joint actuators are position controlled, medium-torque servo-motors with a specified maximum angular velocity of 315°/sec, and an maximum angular velocity in water (observed) of 45°/sec, which enables 0.5 Hz operation for the robot. The robot operates for approximately 20 minutes using a 600mAh battery.

Once the optimal gaits were computed, we store their shape trajectories in the PC. These gaits were radio-transmitted to the eel. We perform our optimal experiments using a fixed, digital camera to record the behavior of the robot in a pool of still water. Image processing is performed off-line, in real-time using the Matrox Imagining Library by a custom-designed multi-tasking software system based on the *LiveObject* architecture for mobile robotics, presented in [15]. We use edge detection, followed by a closing operation to locate the robot as a single blob in the image. The robot's position and orientation in the image plane are determined from the centroid and orientation of this blob. Once data is available in the image plane, the position of fixed landmarks in the image yields a ***homography*** that we use to map the position and orientation of the robot from image plane coordinates into a real-world coordinate frame.

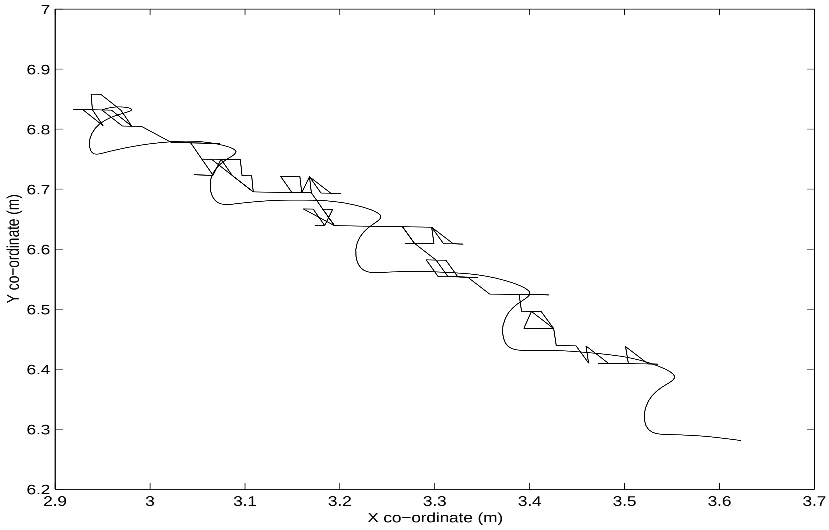

Figure 11: Matching of the optimal forward motion of Fig. 4 with experimental data

Our mathematical model of the eel in water leads to three non-dimensional parameters that influence the dynamics in water: the inertia parameter, $\bar{J}$, and the drag parameters corresponding to the perpendicular and parallel friction forces, $\bar{\mu}^{\perp}$ and $\bar{\mu}^{\|}$ respectively. We tuned these drag parameters using data from one experiment until our simulations matched the observed data. We estimated the dimensional parameters to be $\mu^{\perp} = 0.35$ and $\mu^{\|} = 0.15$. We were then able to use these same values for the drag parameters to match the observed data from all experiments, except for one case (turning in place swimming) which we will describe below.

An important limitation we have found in the implementation of several optimal gaits has been that the REEL II cannot surpass $\pm 45^o$ or $\pm\pi/4$ radians in any of its joint angles due to technical reasons related with the mounting of the individual joint motors, a fact that directly eliminates the possibility of implementing in the pool several of the gaits proposed above. The matching of both simulations and experiments, however, yielded

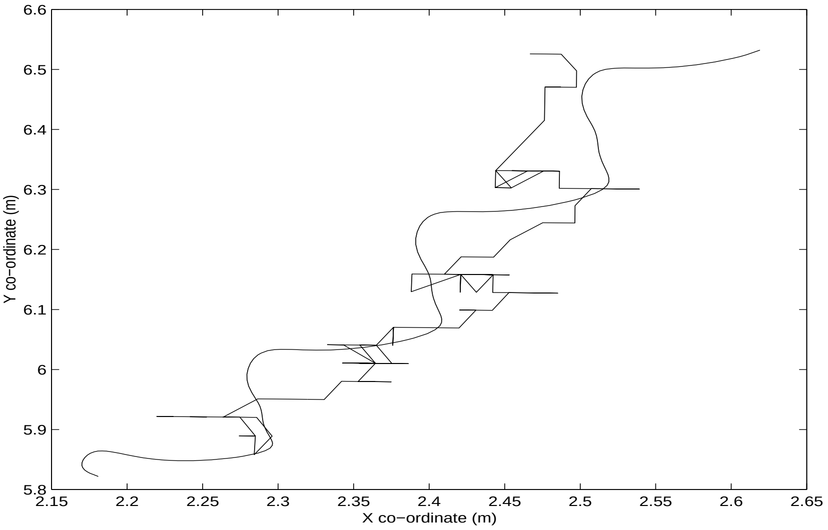

Figure 12: Matching of the optimal forward motion of Fig. 5 with experimental data

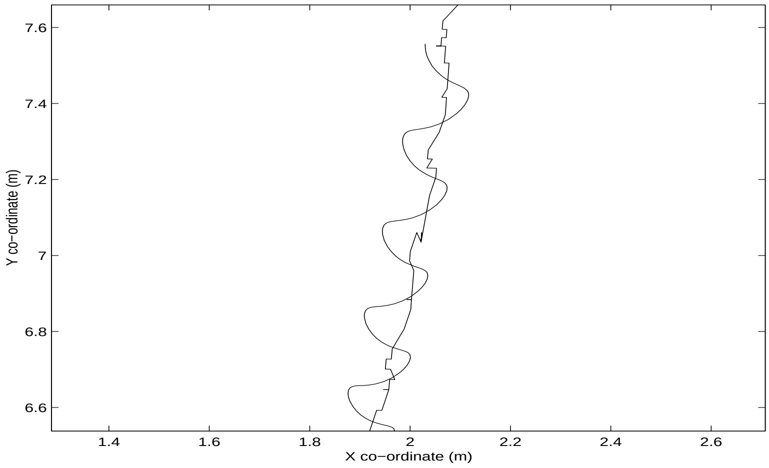

Figure 13: Matching of the optimal forward motion of Fig. 6 with experimental data

quite satisfactory results. We carried out experiments for the optimal gaits found in Section 5.1: forward motion with zero initial and final momentum gait (Fig. 11), building up momentum gait (Fig. 12) and the comparison with the traveling wave gait (Fig. 13), and in Section 5.2: the comparison with the traveling wave (Fig. 14), although we could not test the gait in Fig. 8 because it violated the 45^o actuator limits, so we implemented instead one of the gaits found during the iteration of the Basis Algorithm.

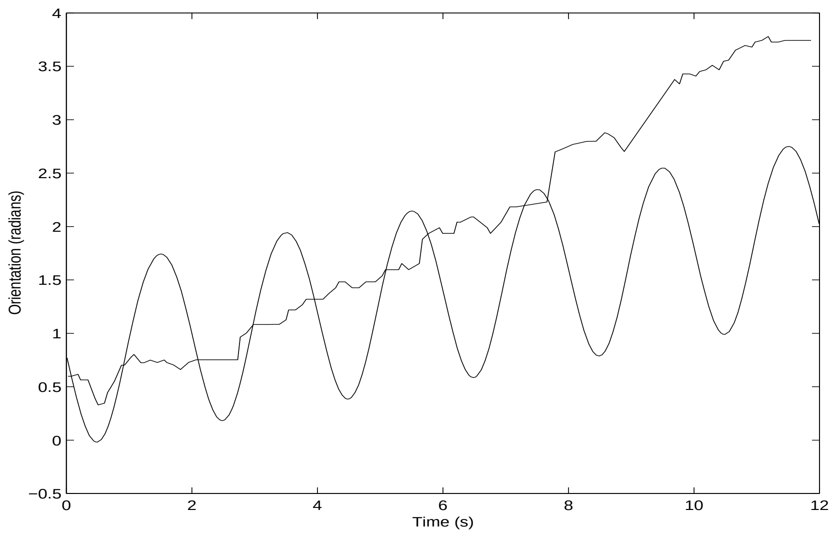

Figure 14: Matching of the one of the spinning gaits found in the iteration to obtain the optimal one (see Fig. 8) with experimental data

It should be noted that since the process of extracting experimental data from video images captures the centroid and the orientation of the major axis of the body of the eel, we do not expect exact overlap of the data. Generally, the simulation results, which show the position and orientation of the center of the mass of the middle link *only*, will generally fluctuate more, centered on the experimental data.

The only gait that showed a marked mismatch between experiment and simulation was the pure rotation gait, as shown in Fig. 14. The rotation accomplished in the experiment turned out to be *larger* than predicted by the model. We attribute the gain in the experimental data to added mass effects of the water that we did not take into account in our model for the eel.

6 Discussion and Conclusion

We have proposed and demonstrated in practice a simple computational procedure for generating near-optimal inputs for an eel-like robot. These techniques have good potential for use in other dynamic robotic locomotion systems, as well as general nonlinear control systems with drift. We have focused on using a truncated basis of sinusoidal inputs so that the optimal energy over this class of inputs can easily be computed. We also showed that in the limit as this basis is made complete, the solution found by our procedure approaches the true optimal solution. Although we have not shown that our truncated basis can necessarily generate any desired final state, we have found in practice that solutions can be obtained using very few terms, and often only one sinusoid for each joint angle was necessary. Further research in this area would be necessary to understand more completely what the minimal basis should be in order to guarantee this for any given system.

In general our experimental work showed good agreement with the simulations. We were able to implement both the forward motion and the rotational motions in the eel. These matched qualitatively the simulations quite well, and we note particularly that the optimal inputs for the turning in place motions were much better than those generated using the analytic approach of [39]. Of course, since we are using a model-based approach to optimize the system, we expect that the experimental results will only be as good as our model. With the very crude fluid drag and actuator model that is used, some potential limitations may arise. For example, we note that we did not have good success in implementing optimal solutions that had significant high frequency components. This is due to the fact that the actuators on the eel could not always track the fastest motions of the inputs. For this reason, we also tested the optimal inputs with fewer harmonics, with generally good results. Also, the effect of changing the parallel frictional parameter can have a significant impact on the shape of the input motions. Thus, if this parameter is not correct (or inappropriately models the effect of parallel drag), the resulting near-optimal solutions will not be correct. However, we found that the experimental results using our estimated parameters were close to those predicted by the model.

We note that although this computational approach is generally easier to implement and has better convergence properties than our previous work [50], there do appear to be certain limitations to this method. For example, it is unlikely that these tools could be applied to general motion planning procedures involving inequality constraints, such as those found in obstacle avoidance or given by actuator constraints. This was seen in our attempts to implement the lateral motions in our experiments, where the necessary input angles for the eel far exceeded the limitations of the REEL II robot. Limiting joint angles could most likely be incorporated into the optimization routines (e.g., by placing conservative limits on the α's), but we have not attempted to do so here.

It is important to emphasize, though, that the implementation and real-time solution of these near-optimal gaits was much more readily done, even for the complex dynamics of the five-link eel, than through other methods we have explored in the past. These techniques thus provide an excellent method for solving for unconstrained motion plans for complex dynamic systems. They can also be used to generate discrete modes, such as forward, rotation, etc., that could be used by a higher level planner in a hierarchical motion planning strategy.

Acknowledgments

The research of J. Cortés and S. Martínez was partially supported by FPU and FPI grants from the Spanish Ministerio de Educación y Cultura and grant DGICYT PB97-1257; and the research of J.P. Ostrowski and K.A. McIsaac was partially supported by NSF grants IRI-9711834, IIS-9876301 and ECS-0086931, and ARO grant DAAH04-96-1-0007.

References

[1] R. Abraham, J.E. Marsden: *Foundations of Mechanics*. 2^{nd} ed., Benjamin-Cummings, Reading (Ma), 1978.

[2] R.McN. Alexander: The gaits of bipedal and quadrupedal animals. *Int. J. Robot. Res.* **3** (2) (1984), 49-59.

[3] R.McN. Alexander: Optimization of gaits in the locomotion of vertebrates. *Physiological Review* **69** (1989), 1199-1227.

[4] J. Baillieul: Geometric methods for nonlinear optimal control problems. *J. Optim. Theory Appl.* **25** (4) (1978), 519-548.

[5] D.J. Balkcom, M.T. Mason: Graphical construction of time optimal trajectories for differential drive robots. *Workshop on Algorithmic Foundation of Robotics (WAFR)*, Dartmouth, USA, 2000, to appear.

[6] A.M. Bloch, P.S. Krishnaprasad, J.E. Marsden, R.M. Murray: Nonholonomic mechanical systems with symmetry. *Arch. Rational Mech. Anal.* **136** (1996), 21-99.

[7] A.M. Bloch, P.S. Krishnaprasad, J.E. Marsden, G. Sánchez de Álvarez: Stabilization of rigid body dynamics by internal and external torques. *Automatica* **28** (1992), 745-756.

[8] R.W. Brockett: Control theory and singular Riemannian geometry. In *New Directions in Applied Mathematics*, eds. P.J. Hilton and G.S. Young, Springer-Verlag, New York, 1982, 11-27.

[9] R.W. Brockett, L. Dai: Nonholonomic kinematics and the role of elliptic functions in constructive controllability. In *Nonholonomic Motion Planning*, eds. Z. Li and J.F. Canny, Kluwer, 1993, 1-21.

[10] F. Bullo, N.E. Leonard, A.D. Lewis: Controllability and motion algorithms for underactuated Lagrangian systems on Lie groups. *IEEE Trans. Automat. Control* **45** (8) (2000), 1437-1454.

[11] G.S. Chirikjian, J.W. Burdick: The kinematics of hyper-redundant locomotion. *IEEE Trans. Robot. Automat.* **11** (6) (1995), 781-793.

[12] J. Cortés, S. Martínez: Optimal control for Nonholonomic Systems with Symmetry. *Proc. IEEE Int. Conf. Decision&Control*, Sydney, Australia, 2000, 5216-5218.

[13] J. Cortés, S. Martínez, J.P. Ostrowski: Motion planning for dynamic locomotion systems: The snakeboard example. In preparation.

[14] J. Cortés, S. Martínez, J.P. Ostrowski, H. Zhang: Simple mechanical control systems with constraints and symmetry. Submitted to *SIAM J. Control Optim.*

[15] A.K. Das, R. Fierro, J.P. Ostrowski, J. Spletzer, C.J. Taylor: A framework for vision based formation control. Submitted to *Multi-Robot Systems: A Special Issue of IEEE Trans. Robot. Automat.*, 2001.

[16] F. Delcomyn: Insect locomotion on land. In *Locomotion and Energetics in Arthropods*, eds. C.F. Herreid II and C.R. Fourtner, Plenum Press, New York, 1981.

[17] J.P. Den Hartog: Forced vibrations with combined Coulomb and viscous friction. *Trans. Amer. Soc. Mech. Engineer.* APM-53-9, 1931.

[18] J. Desai, V. Kumar: Nonholonomic motion planning of cooperating mobile robots. *Proc. IEEE Int. Conf. Robot.&Automat.*, Albuquerque, New Mexico, 1997, 3409-3414.

[19] L.E. Dubins: On curves of minimal length with a constraint on average curvature and with prescribed initial and terminal positions and tangents. *Amer. J. Math.* **79** (1957), 497-516.

[20] O. Ekeberg: A combined neuronal and mechanical model of fish swimming. *Bio. Cyber.* **69** (1993), 363-374.

[21] C. Fernandes, L. Gurvits, Z.X. Li: Optimal nonholonomic motion planning for a falling cat. In *Nonholonomic Motion Planning*, eds. Z. Li and J.F. Canny, Kluwer, 1993.

[22] C. Fernandes, L. Gurvits, Z.X. Li: Near-optimal nonholonomic motion planning for a system of coupled rigid bodies. *IEEE Trans. Automat. Control* **39** (3) (1994), 450-463.

[23] T. Fukuda, A. Kawamoto, F. Arai, H. Matsuura: Steering mechanism of underwater micro mobile robot. *Proc. IEEE Int. Conf. Robot.& Automat.*, Nagoya, Japan, 1995, 363-368.

[24] P. Gambaryan: *How Mammals Run: Anatomical Adaptations*. John Wiley &Sons, New York, 1974.

[25] S. Hirose. *Biologically Inspired Robots: Snake-like Locomotors and Manipulators*. Oxford University Press, Oxford, 1993.

[26] S.D. Kelly, R.M. Murray: Geometric phases and robotic locomotion. *J. Robotic Systems* **12** (6) (1995), 417-431.

[27] S.D. Kelly, R.M. Murray: The geometry and control of dissipative systems. *Proc. IEEE Int. Conf. Decision&Control*, Kobe, Japan, 1996.

[28] H.K. Khalil: *Nonlinear Systems*. 2^{nd} ed., Prentice Hall, Englewood Cliffs, NJ, 1995.

[29] J. Koiller, K. Ehlers, R. Montgomery: Problems and progress in microswimming. *J. Nonlinear Sci.* **6** (1996), 507-541.

[30] W.S. Koon, J.E. Marsden: Optimal control for holonomic and nonholonomic mechanical systems with symmetry and Lagrangian reduction. *SIAM J. Control Optim.* **35** (1997), 901-929.

[31] P.S. Krishnaprasad: Geometric phases and optimal reconfiguration for multibody systems. *Proc. American Control Conference*, Philadelphia, USA, 1990, 2440-2444.

[32] P.S. Krishnaprasad, R. Yang, W. Dayawansa: Control problems on principal bundles and nonholonomic mechanics. *Proc. IEEE Int. Conf. Decision&Control*, 1991, 1133-1138.

[33] J-P. Laumond, P. Jacobs, M. Taix, R. M. Murray: A motion planner for nonholonomic mobile robots, *IEEE Trans. Robot. Automat.* **10** (5) (1994), 577-593.

[34] N.E. Leonard: Periodic forcing, dynamics and control of underactuated spacecraft and underwater vehicles. *Proc. IEEE Int. Conf. Decision&Control*, New Orleans, USA, 1995, 1131-1136.

[35] N.E. Leonard, P.S. Krishnaprasad: Motion control of drift-free, left-invariant systems on Lie groups. *IEEE Trans. Automat. Control* **40** (9) (1995), 1539-1554.

[36] A.D. Lewis, J.P. Ostrowski, R.M. Murray, J.W. Burdick: Nonholonomic mechanics and locomotion: The snakeboard example. *Proc. IEEE Int. Conf. Robot.&Automat.*, San Diego, 1994, 2391-2397.

[37] J.E. Marsden, T.S. Ratiu: *Introduction to Mechanics and Symmetry*. Springer-Verlag, New York, 1994.

[38] K.A. McIsaac: *A hierarchical approach to motion planning with applications to an underwater eel-like robot*. Ph.D thesis, University of Pennsylvania, Philadelphia, 2001.

[39] K.A. McIsaac, J.P. Ostrowski: A geometric approach to anguilliform locomotion: Simulation and experiments with an underwater eel-robot. *Proc. IEEE Int. Conf. Robot.&Automat.*, Detroit, Michigan, 1999, 2843-2848.

[40] K.A. McIsaac, J.P. Ostrowski: Steering algorithms for dynamic robotic locomotion systems. *Workshop on the Algorithmic Foundation of Robotics (WAFR)*, eds. B.R. Donald, K.M. Lynch, D. Rus, Dartmouth, USA, 2001, pp. 221-231.

[41] K.A. McIsaac, J.P. Ostrowski: Open-loop Verification of Motion Planning for an Underwater Eel-like Robot. *Experimental Robotics VII*, Lecture Notes in Control and Information Sciences 271, eds. D. Rus, S. Singh, Honolulu, 2001, pp. 271-280.

[42] R. Montgomery: Isoholonomic problems and some applications. *Comm. Math. Phys.* **128** (1990), 565-592.

[43] R.M. Murray, S.S. Sastry: Nonholonomic motion planning: Steering using sinusoids. *IEEE Trans. Automat. Control* **38** (5) (1993), 700-716.

[44] Y. Nakamura, R. Mukherjee: Exploiting nonholonomic redundancy of free-flying space robots. *IEEE Trans. Robot. Automat.* **9** (4) (1993), 499-506.

[45] J.P. Ostrowski: *The Mechanics and Control of Undulatory Robotic Locomotion*. Ph.D thesis, California Institute of Technology, Pasadena, CA, 1995.

[46] J.P. Ostrowski: Optimal controls for kinematic systems on Lie groups. IFAC World Congress, Beijing, China, 1999.

[47] J.P. Ostrowski: Computing reduced equations for mechanical systems with constraints and symmetries. *IEEE Trans. Robot. Automat.* **15**(1) (1999), 111-123.

[48] J.P. Ostrowski, J.W. Burdick: Controllability tests for mechanical systems with symmetries and constraints. *J. Appl. Math. Comp. Sci.* **7** (2) (1997), 101-127.

[49] J.P. Ostrowski and J.W. Burdick: The geometric mechanics of undulatory robotic locomotion. *Int. J. Robot. Res.* **17** (7) (1998), 683-702.

[50] J.P. Ostrowski, J.P. Desai, V. Kumar: Optimal gait selection for nonholonomic locomotion systems. *Int. J. Robot. Res.* **19** (3) (2000), 225-237.

[51] J.A. Reeds, L.A. Shepp: Optimal paths for a car that goes both forwards and backwards. *Pacific J. Math.* **145** (2) (1990), 367-393.

[52] S. Sastry, R. Montgomery: The structure of optimal controls for a steering problem. *IFAC Symposium on Nonlinear Control Systems Design (NOLCOS)*, Bordeaux, France, 1992.

[53] H.J. Sussmann: A general theorem on local controllability. *SIAM J. Control Optim.* **25** (1) (1987), 158-194.

[54] H.J. Sussmann, G. Tang: Shortest paths for the Reeds-Shepp car: A worked out example of the use of geometric techniques in nonlinear optimal control. Technical report SYCON-91-10, Rutgers University, 1991.

[55] A.E. Taylor, D.C. Lay: *Introduction to functional analysis.* 2^{nd} edition, John Wiley &Sons, New York, 1980.

[56] G.C. Walsh, R. Montgomery, S. Sastry: Optimal path planning on matrix Lie groups. Preprint, 1994.

[57] M. Zefran, J.P. Desai, V. Kumar: Continuous motion plans for robotic systems with changing dynamic behavior. *Workshop on Algorithmic Foundations of Robotics (WAFR)*, Toulouse, France, 1996.

[58] H. Zhang, J.P. Ostrowski: Control algorithms using affine connections on principal fiber bundles. IFAC Workshop on Lagrangian and Hamiltonian methods for Nonlinear Control, Princeton, 2000.

Appendix

Proof of Lemma 4.5

Take $\gamma > 0$. Since $\phi(\delta)$ is continuous, there exits $\epsilon > 0$ such that for all $\epsilon \leq \epsilon_0$, $\|\phi(\delta+\epsilon)-\phi(\delta)\| < \gamma$. Then, $\phi(\delta+\epsilon_0) < \gamma + \phi(\delta)$. Assume $\|u\|_2 < \delta$. For ϵ_0, there exists k_0 such that if $k \geq k_0$, $\|u_k\|_2 \leq \|u\|_2 + \epsilon_0 < \delta + \epsilon_0$. Thus, from the BIBS stability, we deduce that

$$\|z_k\|_{C[0,T]} < \phi(\delta+\epsilon_0) < \gamma + \phi(\delta)\,,\ \forall k \geq k_0\,.$$

$\boxed{QED}$

Proof of Lemma 4.6

Denote by $\bar{z}_k(t)$ the difference $\bar{z}_k(t) = z_k(t) - z(t)$. We have

$$\dot{\bar{z}}_k(t) = f(z_k(t)) - f(z(t)) + B(z_k(t))\,(u_k(t)-u(t)) + (B(z_k(t)) - B(z(t)))\,u(t)\,,$$

which implies

$$\begin{aligned}\|\dot{\bar{z}}_k(t)\|_{\mathbb{R}^d} \leq{}& \|f(z_k(t)) - f(z(t))\|_{\mathbb{R}^d} + \|B(z_k(t))\|_{\mathbb{R}^{d\times m}}\|u_k(t)-u(t)\|_{\mathbb{R}^m}\\ &+ \|B(z_k(t)) - B(z(t))\|_{\mathbb{R}^{d\times m}}\|u(t)\|_{\mathbb{R}^m}\,. \end{aligned} \tag{22}$$

By the mean value theorem (see [28]), we have that

$$|f^i(z_k) - f^i(z)| = \Big|\frac{\partial f^i}{\partial z}(c_k^i)\cdot(z_k - z)\Big| \leq \Big\|\frac{\partial f^i}{\partial z}(c_k^i)\Big\|_{\mathbb{R}^d}\|z_k - z\|_{\mathbb{R}^d}\,,\ 1 \leq i \leq d\,,$$

where $c_k^i(t)$ belongs to the segment in $\mathbb{R}^d$ joining $z_k(t)$ and $z(t)$. Then,

$$\|f(z_k) - f(z)\|_{\mathbb{R}^d} \leq \sqrt{d} \max_{1\leq i\leq d} \Big\| \frac{\partial f^i}{\partial z}(c_k^i) \Big\|_{\mathbb{R}^d} \|z_k - z\|_{\mathbb{R}^d} .$$

Now,

$$\begin{aligned}\|c_k^i(t)\|_{\mathbb{R}^d} &\leq \max_{1\leq i\leq d} \|c_k^i(t)\|_{\mathbb{R}^d} \leq \max_{1\leq i\leq d} \{\|z_k(t)\|_{\mathbb{R}^d}, \|z(t)\|_{\mathbb{R}^d}\} \\ &\leq \max_{1\leq i\leq d} \big\{\|z_k(t)\|_{C[0,T]}, \|z(t)\|_{C[0,T]}\big\} \leq \gamma_0 + \phi(\delta)\,, \ \ \forall k \geq k_0\,,\end{aligned}$$

where we have used Lemma 4.5 in the last inequality. Otherwise said, we have that for $k \geq k_0$, the $c_k^i(t)$ belong to the compact set $B(0, \gamma_0 + \phi(\delta))$ for all i. Since $\frac{\partial f^i}{\partial z}$ is continuous for $1 \leq i \leq d$, we have that $\|\frac{\partial f^i}{\partial z}\|_{\mathbb{R}^d} < K_i$ over $B(0, \gamma_0 + \phi(\delta))$ for some constant K_i. Therefore

$$\|f(z_k) - f(z)\|_{\mathbb{R}^d} \leq C_1 \|z_k - z\|_{\mathbb{R}^d}\,, \ \ \forall k \geq k_0\,,$$

with $C_1 = \sqrt{d} \max\limits_{1\leq i\leq d} K_i$.

Similarly, we can prove that there exist constants C_2, $C_3 > 0$ such that

$$\begin{aligned}\|B(z_k) - B(z)\|_{\mathbb{R}^{d\times m}} &\leq C_2 \|z_k - z\|_{\mathbb{R}^d}\,, \\ \|B(z_k)\|_{\mathbb{R}^{d\times m}} &\leq C_3\,,\end{aligned}$$

for all $k \geq k_0$. Substituting in Eq. 22, we get

$$\begin{aligned}\|\dot{\bar{z}}_k(t)\|_{\mathbb{R}^d} &\leq C_1 \|\bar{z}_k(t))\|_{\mathbb{R}^d} + C_2 \|\bar{z}_k(t))\|_{\mathbb{R}^d} \|u(t)\|_{\mathbb{R}^m} + C_3 \|u_k(t) - u(t)\|_{\mathbb{R}^m} \\ &= (C_1 + C_2 \|u(t)\|_{\mathbb{R}^m})\, \|\bar{z}_k(t))\|_{\mathbb{R}^d} + C_3 \|u_k(t) - u(t)\|_{\mathbb{R}^m}\,,\ \forall k \geq k_0\,.\end{aligned}$$

Denote by $\psi_1(t) = C_1 + C_2 \|u(t)\|_{\mathbb{R}^m}$ and $\psi_2(t) = C_3 \|u_k(t) - u(t)\|_{\mathbb{R}^m}$, and for each $k \geq k_0$ let us set up the equation:

$$\begin{cases} \dot{q}_k = \psi_1(t) q_k + \psi_2(t) \\ q_k(0) = 0\,. \end{cases}$$

By Lemma 2.5 in [28], we conclude that $\|\bar{z}_k(t)\|_{\mathbb{R}^d} \leq q_k(t)$. Integrating the equation for $q_k(t)$, applying Hölder inequality and taking the maximum in $t \in [0, T]$, we finally obtain

$$\|z_k(t) - z(t)\|_{C[0,T]} \leq L \|u_k - u\|_2\,,\ \forall k \geq k_0\,,$$

where L is a constant depending on γ_0 and $\|u\|_2$. $\boxed{QED}$

Proof of Theorem 4.4

As we see below, the proof of the theorem in [22] remains valid under the application of the precedent lemmas. For the sake of completeness we review it here.

The proof consists of two parts. First, consider the following problems

$$P_{\infty,\gamma} : \dot{z} = f(z) + B(z)u\,, \quad z_0\,, z_f \in \mathbb{R}^d\,, \quad u(t) = \sum_{i=1}^{\infty} \alpha_i \mathbf{e}_i(t)\,,$$

with cost function and minimum cost, respectively

$$\mathcal{J}_{\infty,\gamma}(\alpha) = \sum_{i=1}^{\infty} \alpha_i^2 + \gamma \|z(T) - z_f\|^2_{\mathbb{R}^d}\,, \quad \mathcal{J}_{\infty,\gamma} = \min_{\alpha}(\mathcal{J}_{\infty,\gamma}(\alpha))\,.$$

Now, we are going to prove that

$$\mathcal{J}_{\infty,\gamma} \longrightarrow \mathcal{J}_*\,, \quad d(S_{\infty,\gamma}, S_*) \longrightarrow 0\,, \text{ as } \gamma \to +\infty\,.$$

In fact, consider the sequence of solutions $\{(z_p, u_p) \in S_{+\infty,\gamma_p}\}$ associated to $\{\gamma_p\}_{p=1}^{+\infty}$ such that $\gamma_p \to +\infty$ as $p \to +\infty$. Then, it can be checked that

$$\|u_p\|_2^2 \le \mathcal{J}_{\infty,\gamma_p} \le \mathcal{J}_{\infty,\infty} \equiv \mathcal{J}_* < +\infty\,, \tag{23}$$

$$\gamma_p \|z_p(T) - z_f\|^2_{\mathbb{R}^d} \le \mathcal{J}_* < +\infty\,, \ \forall p\,. \tag{24}$$

Since $L_2[0,T]$ is a reflexive space and because of Eq. 23, there exists a subsequence $\{u_{p_l}\}_{l=1}^{\infty} \subseteq \{u_p\}_{p=1}^{\infty}$ which is weakly convergent to some $u \in L_2[0,T]$ with $\|u\|_2^2 \le \mathcal{J}_*$, (see Th. 10.6 in [55]). In fact, since $\mathcal{J}_*$ is a minimum, necessarily $\|u\|_2^2 \equiv \mathcal{J}_*$ and then $\|u_{p_l} - u\|_2 \to 0$, as $l \to \infty$. By Lemma 4.6, we deduce

$$\|z_{p_l} - z\|_{C[0,T]} \longrightarrow 0\,, \text{ as } l \to \infty\,,$$

where z is the solution of Eq. 17 corresponding to u. On the other hand, using Eq. 23 and the convergence seen for $\{u_{p_l}\}$, $\{z_{p_l}\}$, we have that $z(T) = z_f$ and $\mathcal{J}_{\infty,\gamma_{p_l}} \to \mathcal{J}_*$ as $l \to +\infty$. In particular, $(z,u) \in S_*$ and $d(S_{\infty,\gamma_{p_l}}, S_*) \to 0$ as $l \to +\infty$.

To complete the proof, it remains to show that $\mathcal{J}_{N,\gamma} \to \mathcal{J}_{\infty,\gamma}$ and $d(S_{N,\gamma}, S_{\infty,\gamma}) \to 0$ as $N \to \infty$ and γ remains fixed.

It is clear that $\mathcal{J}_{N+1,\gamma} \le \mathcal{J}_{N,\gamma} \le \mathcal{J}_{1,\gamma}$, for all N, and thus

$$\lim_{N\to\infty} \mathcal{J}_{N,\gamma} \ge \mathcal{J}_{\infty,\gamma}\,.$$

Let (z,u) be a solution in $S_{\infty,\gamma}$, where $u(t) = \sum_{i=1}^{\infty} \alpha_i \mathbf{e}_i(t)$. Define for each $k \in \mathbb{N}$

$$u_k(t) = \sum_{i=1}^{k} \alpha_i \mathbf{e}_i(t)\,,$$

and consider the solutions of $\dot{z}_k = f(z_k) + B(z_k)u_k$, $z_k(0) = z_0$. By how we have chosen the inputs $u_k(t)$, it is straightforward that $\|u_k - u\|_2 \to 0$ as $k \to \infty$. Then, again by Lemma 4.6,

$$\|z_k - z\|_{C[0,T]} \to 0\,, \text{ as } k \to \infty\,.$$

Since

$$\mathcal{J}_{k,\gamma} \leq \mathcal{J}_{k,\gamma}(z_k, u_k) \leq \mathcal{J}_{\infty,\gamma} + \delta_k \,,$$

where $\delta_k = \gamma \|z_k(T) - z_f\|^2_{\mathbb{R}^d} \to 0$ as $k \to \infty$, we have that $\lim_{k\to\infty} \mathcal{J}_{k,\gamma} = \mathcal{J}_{\infty,\gamma}$.

Finally, take any sequence $\{(z_N, u_N) \in S_{N,\gamma}\}_{N=1}^{\infty}$. Since $\{u_N\}_{N=1}^{\infty}$ is bounded in $L_2[0,T]$ (cf. Eq. 23), there exists a subsequence $\{(z_{N_k}, u_{N_k})\}_{k=1}^{\infty}$ such that $u_{N_k} \to u$ weakly as $k \to \infty$. Reasoning as in the first part of the proof we have that $\|u_{N_k} - u\|_2 \to 0$ and, by the use of Lemma 4.6, there exists $z \in C[0,T]$ such that

$$\dot{z} = f(z) + B(z)u \,, \quad z(0) = z_0 \,, \quad \text{and} \quad \|z_{N_k} - z\|_{C[0,T]} \to 0 \,, \text{as } k \to \infty \,.$$

Now,

$$\begin{aligned} \|u\|_2^2 + \gamma \|z(T) - z_f\|^2_{\mathbb{R}^d} &= \lim_{k\to\infty} \left(\|u_{N_k}\|_2^2 + \gamma \|z_{N_k}(T) - z_f\|^2_{\mathbb{R}^d} \right) \\ &= \lim_{N_k\to\infty} \mathcal{J}_{N_k,\gamma} = \mathcal{J}_{\infty,\gamma} \,, \end{aligned}$$

and then $(z, u) \in S_{\infty,\gamma}$. $\boxed{QED}$